TITLE: MULTIPLE, REDUNDANT CARBOXYLIC ACID TRANSPORTERS SUPPORT MITOCHONDRIAL METABOLISM IN *PLASMODIUM FALCIPARUM*

Authors: Krithika Rajaram[1,2*], Gabriel W. Rangel[3,4*], Justin T. Munro[4,5], Sethu C. Nair[1], Manuel Llinás[3,4,5#], Sean T. Prigge[1#]

[1] Department of Molecular Microbiology and Immunology, Bloomberg School of Public Health, Johns Hopkins University, Baltimore, MD 21205

[2] Present address: Department of Microbiology, The Ohio State University, Columbus, OH 43210

[3]Department of Biochemistry and Molecular Biology, Pennsylvania State University, University Park, PA 16802

[4] Huck Center for Malaria Research, Pennsylvania State University, University Park, PA 16802

[5] Department of Chemistry, Pennsylvania State University, University Park, PA 16802

[*]Equal Contribution

[#]Corresponding Authors

ABSTRACT:

The mitochondrion of the deadliest human malaria parasite, *Plasmodium falciparum,* is an essential source of cellular acetyl-CoA during the asexual blood-stage of the parasite life cycle. Blocking mitochondrial acetyl-CoA synthesis leads to a hypoacetylated proteome and parasite death. We previously determined that mitochondrial acetyl-CoA is primarily synthesized from glucose-derived pyruvate by α-ketoacid dehydrogenases. Here, we asked if inhibiting the import of glycolytic pyruvate across the mitochondrial inner membrane would affect acetyl-CoA production and, thus, could be a potential target for antimalarial drug development. We selected the two predicted mitochondrial pyruvate carrier proteins (*Pf*MPC1 and *Pf*MPC2) for genetic knockout and isotopic metabolite tracing via HPLC-MS metabolomic analysis. Surprisingly, we observed that asexual blood-stage parasites could survive the loss of either or both *Pf*MPCs with only minor growth defects, despite a substantial reduction in the amount of glucose-derived isotopic labelling into acetyl-CoA. Furthermore, genetic deletion of two additional mitochondrial

carboxylic acid transporters – DTC (di/tricarboxylic acid carrier) and YHM2 (a putative citrate/α-ketoglutarate carrier protein) – only mildly affected asexual blood-stage replication, even in the context of *Pf*MPC deficiency. Although we observed no added impact on the incorporation of glucose carbon into acetyl-CoA in these quadruple knockout mutants, we noted a large decrease in glutamine-derived label in tricarboxylic acid cycle metabolites, suggesting that DTC and YHM2 both import glutamine derivatives into the mitochondrion. Altogether, our results expose redundant routes used to fuel the blood-stage malaria parasite mitochondrion with imported carbon from two major sources – glucose and glutamine.

SIGNIFICANCE:

The mitochondrion of malaria parasites generates key molecules, such as acetyl-CoA, that are required for numerous cellular processes. To support mitochondrial biosynthetic pathways, the parasites must transport carbon sources into this organelle. By studying how the mitochondrion obtains pyruvate, a molecule derived from glucose, we have uncovered redundant carbon transport systems that ensure parasite survival in red blood cells. This metabolic redundancy poses a challenge for drug development, as it enables the parasite to adapt and survive by relying on alternative pathways when one is disrupted.

INTRODUCTION:

Plasmodium falciparum is a protozoan parasite that causes the deadliest form of malaria in humans, killing over 600,000 people annually (World Health Organization, 2023). Each malaria parasite contains a single mitochondrion that is required throughout its life cycle. Despite its essentiality, only a few critical functions have been attributed to the mitochondrion during the symptomatic stage of disease when parasites largely replicate asexually within human red blood cells. The tricarboxylic acid (TCA) cycle is dispensable in the asexual blood stage (ABS) forms (Ke et al., 2015; Rajaram et al., 2022), and the primary purpose of the mitochondrial electron transport chain (mETC) is to furnish ubiquinone for dihydroorotate dehydrogenase (DHODH), a mitochondrial enzyme that participates in *de novo* pyrimidine synthesis (Painter et al., 2007). As a result, nearly all mitochondrial-specific antimalarials have been developed to target either the

59 mETC or DHODH. However, in sexual blood-stage parasites, other mitochondrial enzymes are
60 critical to development including aconitase (Ke et al., 2015) and isocitrate dehydrogenase (Yang
61 et al., 2022). To expand the druggable mitochondrial proteome, the organelle has been the focus
62 of intense research to further our understanding of its biology and metabolic output.

63 In line with these efforts, we recently established that the *P. falciparum* mitochondrion is
64 responsible for generating cellular acetyl-CoA in ABS parasites (Nair et al., 2023). This production
65 is largely driven by mitochondrial pyruvate dehydrogenase (mPDH), also known as the branched
66 chain alpha-keto acid dehydrogenase. The multisubunit mPDH complex uses glucose-derived
67 carbon, likely in the form of pyruvate, a three-carbon carboxylic acid product of glycolysis, as its
68 substrate. Although a second PDH complex exists in the apicoplast organelle in *Plasmodium*, it is
69 dispensable in ABS parasites (Cobbold et al., 2013; Pei et al., 2010; Swift et al., 2020a). When
70 mPDH is disrupted, parasites become reliant on the TCA cycle enzyme α-ketoglutarate
71 dehydrogenase (KDH) for survival. KDH is an α-ketoacid dehydrogenase that is closely related to
72 mPDH and that primarily converts α-ketoglutarate into succinyl-CoA in parasites; however, *in*
73 *vitro*, it has also been demonstrated to catalyze the conversion of pyruvate to acetyl-CoA (Chan
74 et al., 2013). The two enzymes constitute a synthetic lethal pair, and their inactivation results in
75 the hypoacetylation of histones and other proteins outside the mitochondrion (Nair et al., 2023).

76 A recent study has shown that 5-15% of the cellular acetate pool in mammalian cells is
77 derived from ROS-mediated pyruvate decarboxylation (Liu et al., 2018). While non-enzymatic
78 conversion of pyruvate to acetate may also occur in *Plasmodium* parasites, it is insufficient to
79 sustain parasites lacking functional mPDH and KDH, which instead require supplementation with
80 millimolar quantities of acetate for survival (Nair et al., 2023). A nuclear acetyl-CoA synthetase
81 (ACS) is responsible for scavenging and ligating free acetate to CoA (Nair et al., 2023; Prata et al.,
82 2021; Summers et al., 2021). However, given the high concentration of acetate required for this
83 bypass to be effective, ACS is unlikely to be a significant generator of acetyl-CoA under
84 physiological conditions (Nair et al., 2023). Combined with recent observations that pyruvate and
85 mitochondrial energy metabolism are linked to artemisinin resistance, the acetyl-CoA
86 biosynthetic pathway has emerged as a promising target for drug discovery (Chen et al., 2014; de
87 Vries et al., 2022; Mok et al., 2021; Schalkwijk et al., 2019; Zhang et al., 2022).

88 Pyruvate is generated from the breakdown of glucose during glycolysis and must be
89 imported from the cytoplasm into the mitochondrial matrix for use by mPDH/KDH (Nair et al.,
90 2023). In many eukaryotes, the transport of ions, metabolites and proteins across the outer
91 mitochondrial membrane is mediated by a highly abundant porin called the voltage-dependent
92 anion channel (VAC) (Hodge and Colombini, 1997; Homblé et al., 2012; Mallo et al., 2021;
93 Wideman et al., 2013). *P. falciparum* has a putative VAC that was recently demonstrated to be
94 essential for parasite survival (Anaguano et al., 2023). The protein localizes primarily to a
95 membrane at the parasite-host interface but also appears to overlap partially with the
96 mitochondrion. The inner mitochondrial membrane is far more selective, and entry is typically
97 mediated by specific solute transporters (Cunningham and Rutter, 2020). *P. falciparum* encodes
98 two proteins that are homologous to the mitochondrial pyruvate carrier proteins MPC1 and
99 MPC2 found in yeast, mammals, and the related apicomplexan parasite *Toxoplasma gondii*
100 (Bricker et al., 2012; Herzig et al., 2012; Lyu et al., 2023; Weiner and Kooij, 2016; Wunderlich,
101 2022). These are small proteins (12 kDa and 15 kDa, respectively) that form part of a heteromeric
102 complex of about 150 kDa in other organisms (Bricker et al., 2012; Herzig et al., 2012).
103 In this study, we probed whether the putative MPC proteins in *P. falciparum* (hereafter
104 referred to as *Pf*MPC) play a role in acetyl-CoA synthesis by transporting pyruvate into the
105 mitochondrion. We employed CRISPR-based gene deletion methods to discover that both
106 proteins are in fact dispensable in ABS parasites. However, there is a marked decrease in the
107 incorporation of ^{13}C glucose into acetyl-CoA and its derivatives in *Pf*MPC-deficient parasites,
108 confirming the role of the *Pf*MPCs in pyruvate import. Deletion of two additional carboxylic acid
109 transporters, a mitochondrial di/tricarboxylate carrier (DTC) and a putative citrate/α-
110 ketoglutarate transporter (YHM2), in the parasite line lacking the two *Pf*MPCs did not further
111 impact survival or ^{13}C glucose incorporation into known mitochondrial metabolites but did
112 impact ^{13}C glutamine incorporation into TCA cycle metabolites. Overall, our data indicate that
113 malaria parasites employ redundant mitochondrial carboxylate transporters to fuel the TCA cycle
114 with carbon derived from glucose and glutamine.
115
116 **RESULTS:**

117 **Mitochondrial carrier proteins *Pf*MPC1 and *Pf*MPC2 are dispensable for blood-stage growth of**
118 ***P. falciparum***

119 Pyruvate is conventionally imported into mitochondria for conversion to acetyl-CoA. This
120 process is mediated by members of the mitochondrial pyruvate carrier (MPC) family. While three
121 paralogs of this family have been found in yeast, human and *Plasmodium* genomes only encode
122 two MPC proteins (Bricker et al., 2012; Herzig et al., 2012; Wunderlich, 2022). *Pf*MPC1 and
123 *Pf*MPC2 have been assigned strong localization scores by two different computational methods
124 (MitoProtII and PlasmoMitoCarta) (Claros and Vincens, 1996; van Esveld et al., 2021). To confirm
125 these predictions, we examined the cellular location of the putative *Pf*MPC1 (PF3D7_1340800)
126 and *Pf*MPC2 (PF3D7_1470400) proteins in *P. falciparum* by generating parasite lines with second
127 copies of *Pf*MPC1 or *Pf*MPC2 fused to a C-terminal SFG (superfolder GFP) tag (Pédelacq et al.,
128 2006; Roberts et al., 2019) (**Fig. S1A-D**). Unfortunately, the *Pf*MPC1-SFG signal was too faint to
129 be measured by live-cell imaging and was undetectable by immunofluorescence microscopy.
130 However, an MPC1 homolog in the closely related parasite *T. gondii* has been experimentally
131 established as a mitochondrial protein (Lyu et al., 2023). Live microscopy analysis of the
132 transgenic parasites showed that *Pf*MPC2-SFG colocalized with the MitoTracker probe,
133 confirming that *Pf*MPC2 is a mitochondrial protein (**Fig. 1A**).

134 To determine if *Pf*MPC1 and *Pf*MPC2 have essential roles in blood-stage parasites, we
135 used CRISPR/Cas9 to knock out the genes individually in an NF54^{attB} parasite line (Adjalley et al.,
136 2010) (**Fig. S2**). Successful gene deletions were confirmed by diagnostic PCR (**Fig. 1B-C**), indicating
137 that both proteins are dispensable in ABS parasites. In yeast, MPC1 forms a heteromeric complex
138 with MPC2 or MPC3, and deletion of either participating subunit renders the transporter non-
139 functional (Bender et al., 2015; Tavoulari et al., 2019). However, it has recently been found that
140 homotypic complexes of human MPC2 are capable of transporting pyruvate in the absence of
141 MPC1 (Nagampalli et al., 2018). To determine if one MPC protein can substitute for the other in
142 *P. falciparum*, we attempted to create a double-knockout line by targeting *Pf*MPC1 for deletion
143 in Δ*Pf*MPC2 parasites. To provide a possible metabolic bypass, we divided the transfected
144 parasite culture into two flasks; one flask contained media that was supplemented with 5 mM

acetate in the event that the deletion of both *Pf*MPC proteins blocked all acetyl-CoA production in the mitochondrion.

To our surprise, we obtained parasites lacking *Pf*MPC1 and *Pf*MPC2 (hereafter referred to as Δ2) in media with or without acetate (**Fig. S3A-C**). We compared the growth of Δ2 parasites against the parental line and observed only a moderate ABS fitness defect (**Fig. 1D**). These results suggest that *Pf*MPC1 and *Pf*MPC2 either do not play a major role in supporting acetyl-CoA synthesis in *P. falciparum*, or that a different mechanism is able to partially compensate for their absence.

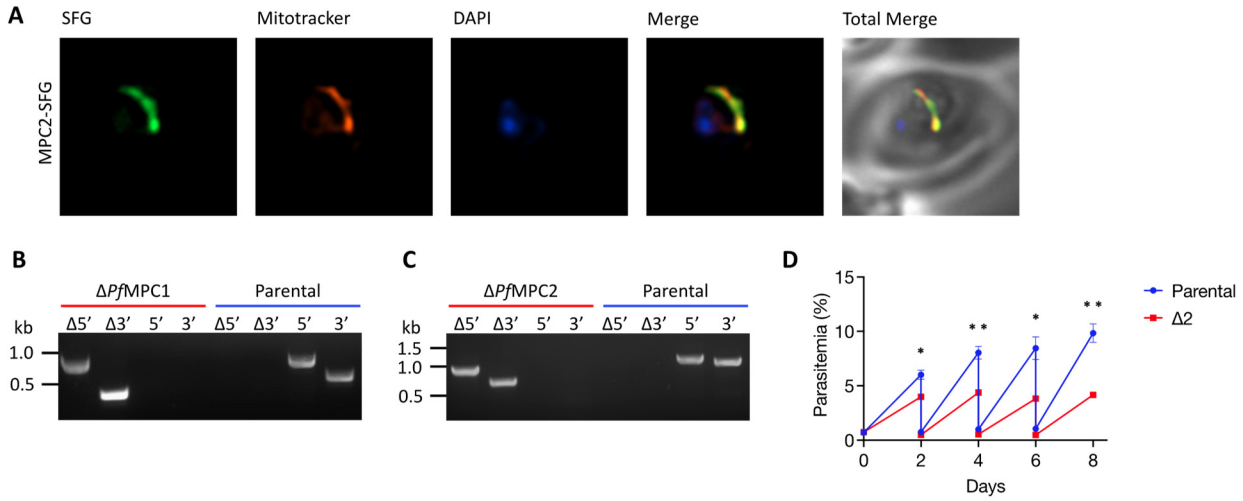

Fig. 1. *Pf*MPC proteins are dispensable in ABS parasites. (A) Representative immunofluorescence microscopy images of *Pf*MPC2-SFG parasites show that *Pf*MPC2-SFG (green) colocalizes with MitoTracker (red) [Mander's coefficient M1 (green in red) = 0.97, SD = 0.015, n = 19]. Images represent fields that are 10 μm long by 10 μm wide. Gene deletion of (B) *Pf*MPC1 and (C) *Pf*MPC2 in NF54^{attB} (parental) parasites was confirmed by PCR amplification (Δ5′ and Δ3′ products). Intact gene loci (5′ and 3′ products) were detected only in the parental (blue) and not in the mutant lines (red). (D) Growth of Δ2 and parental parasites was monitored by flow cytometry over an 8-day period. Cultures were seeded at 0.5% parasitemia on day 0 and diluted 1:8 every other day. Two biological experiments were conducted in quadruplicate (two-way ANOVA computed using Prism 10 [GraphPad Software, Inc], with Šídák's multiple comparison test; *, $p \leq 0.05$; **, $p \leq 0.01$). Error bars represent the standard deviations from the mean.

*Pf*MPCs are required for optimal incorporation of glucose carbon into acetyl-CoA

166 Once pyruvate enters the mitochondrion, it is acted upon by α-ketoacid dehydrogenases
167 to yield the two-carbon-donor compound acetyl-CoA. Acetyl-CoA then enters the TCA cycle by
168 combining with the four-carbon molecule oxaloacetate to form six-carbon citrate. Citrate is
169 converted in two steps to α-ketoglutarate, which also serves as an entry point for carbon derived
170 from glutamine into the TCA cycle (**Fig. 2A**). Our previously published results indicate that acetyl-
171 CoA or an unknown derivative is also exported out of the mitochondrion to acetylate proteins
172 and metabolites in the cytosol and nucleus (Nair et al., 2023). To determine if the levels of acetyl-
173 CoA and downstream products are affected in Δ2 compared to parental parasites, we replaced
174 unlabeled glucose or glutamine in the culture media with isotopically labeled $^{13}C_6$-glucose or $^{13}C_5$-
175 glutamine, respectively, and traced carbon incorporation into various metabolites using HPLC-
176 MS metabolomics (**Fig. 2A**).
177 We found that over 86% of hexose phosphate and over 60% of α-ketoglutarate were
178 derived from ^{13}C-glucose and ^{13}C-glutamine, respectively, over the course of the 2.5-hour labeling
179 period in both parasite lines (**Fig. 2B**, **Fig. S4A**). As expected, the fraction of labeling from ^{13}C-
180 glutamine in TCA cycle intermediates and N-acetyl-glutamate, an acetylated amino acid derived
181 from acetyl-CoA, did not vary significantly between the two lines, ruling out any intrinsic
182 variations in these metabolic pathways between the parental and Δ2 parasites (**Fig. 2C-E**, **Fig. S4**).
183 We next examined the incorporation of ^{13}C label from glucose into acetyl-CoA and N-
184 acetyl-glutamate (**Fig. 2C-D**). In parental parasites, both metabolites were labeled with two
185 carbons from $^{13}C_6$-glucose (M+2); by contrast, this labeling was highly reduced, though not
186 absent, in Δ2 parasites. The integrity of this pathway is also evident from the levels of two-carbon
187 and five-carbon (M+5; with three oxaloacetate carbons derived from anaplerotic sources) labeled
188 citrate species, which are only slightly reduced in Δ2 compared to parental parasites (**Fig. 2E**).
189 Similarly, negligible reductions are observed in the M+2 glucose label in downstream TCA cycle
190 metabolites (**Fig. S4**). These results suggest that *Pf*MPC1 and *Pf*MPC2 are the primary
191 mitochondrial pyruvate carriers, and their loss negatively impacts acetyl-CoA synthesis and
192 parasite growth. Despite this, *Pf*MPC deficiency is not lethal likely because some glucose-derived
193 carbon is still available in the mitochondrion to produce sufficient levels of acetyl-CoA.

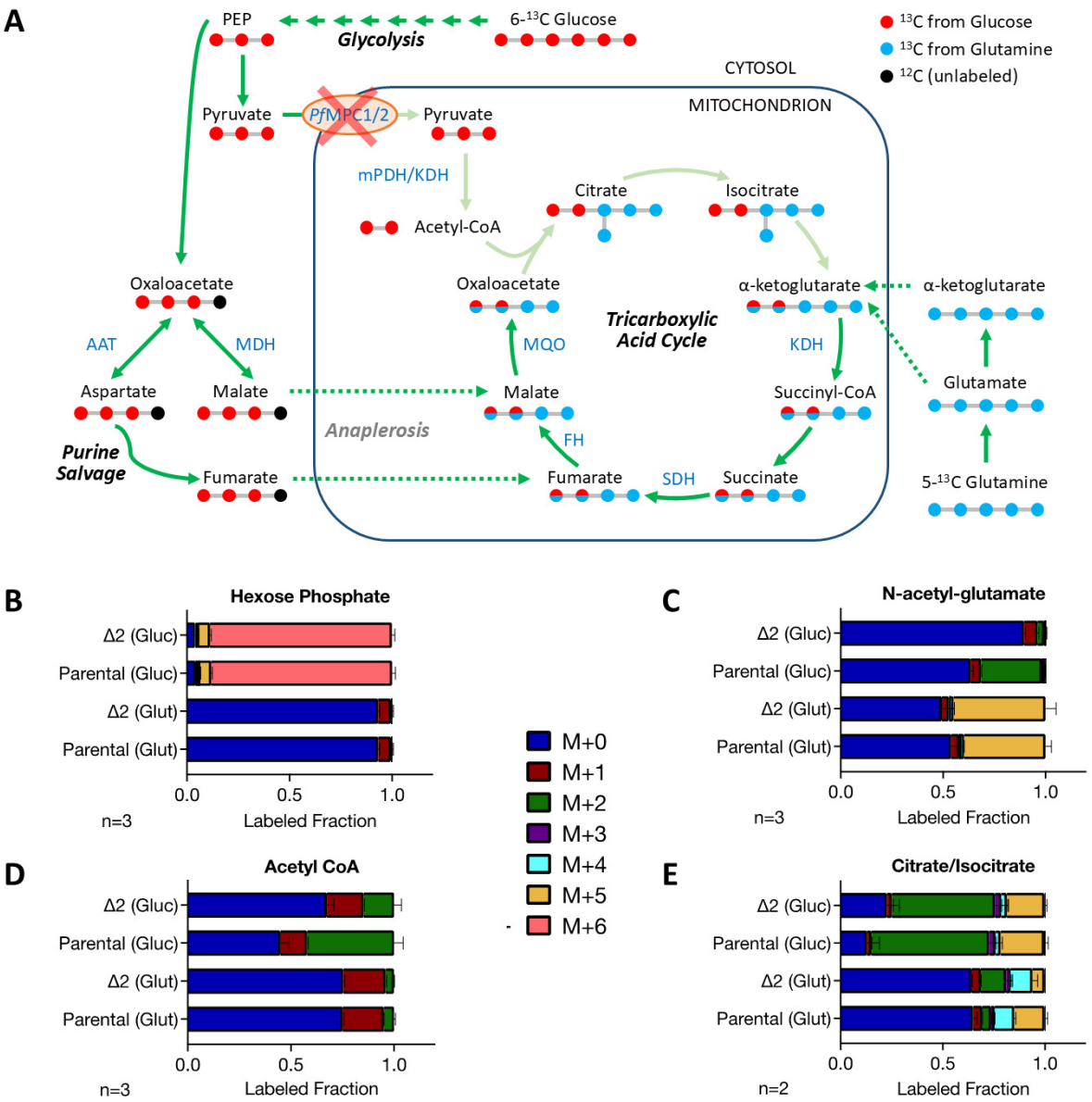

Fig. 2. *Pf*MPC deletion reduces the synthesis of acetyl-CoA from glucose. (A) Schematic depicting the labeling pattern of mitochondrial metabolites in Δ2 parasites after short-term incubation with uniformly labeled ^{13}C-glucose (solid red circles) or ^{13}C-glutamine (solid blue circles). Black circles represent unlabeled atoms. Circles colored with both red and blue indicate carbons that may be derived from either ^{13}C-glucose or ^{13}C-glutamine. Arrows represent enzymatic reactions and are colored based on the known flow (dark green), reduced flow (light green) or predicted flow (dotted green) of carbon atoms. Abbreviations: PEP – phosphoenolpyruvate; AAT – aspartate aminotransferase; MDH – malate dehydrogenase; mPDH –

203 mitochondrial pyruvate dehydrogenase; KDH – α-ketoglutarate dehydrogenase; SDH – succinate
204 dehydrogenase; FH – fumarate dehydrogenase; MQO – malate-quinone oxidoreductase. (B-E) Fraction of
205 isotopically labeled metabolites when parental or Δ2 parasites are incubated with labeled glucose (Gluc)
206 or glutamine (Glut). Color coding denotes the mass (M) of the parent compound plus the mass shift from
207 the incorporation of heavy carbon isotope (^{13}C). Labeling data are expressed as the fraction of the total
208 metabolite pool observed in 'n' independent experiments. Error bars represent the standard deviations
209 from the mean.
210

211 **DTC and YHM2 are dispensable individually and together with *Pf*MPCs**

212 While *Pf*MPC1 and *Pf*MPC2 appear responsible for the vast majority of pyruvate import
213 into the *P. falciparum* mitochondrion, a limited amount of glucose carbon still enters the
214 organelle in their absence (**Fig. 2**, **Fig. S4**). To determine if other mitochondrial carboxylate
215 transporters can substitute for *Pf*MPCs, we searched the annotated *P. falciparum* genome using
216 resources on PlasmodDB.org for putative mitochondrial carboxylate carriers and found two
217 candidates (Alvarez-Jarreta et al., 2024; Aurrecoechea et al., 2009; Harb et al., 2024). The first, a
218 di/tricarboxylic acid transporter (DTC; PF3D7_0823900), is a known mitochondrial protein that
219 has been shown to exchange several carboxylates in reconstituted liposomes (Nozawa et al.,
220 2011; van Dooren et al., 2006); however, its affinity for pyruvate, a monocarboxylate, has not
221 been evaluated. The second candidate, YHM2 (PF3D7_1223800), a homolog of the yeast
222 citrate/α-ketoglutarate transporter, has not been characterized in *P. falciparum* (Castegna et al.,
223 2010). To determine its subcellular location, we generated transgenic parasites expressing a
224 second copy of SFG-tagged YHM2 (**Fig. S1A-B**, **Fig. S5**) and confirmed the colocalization of YHM2-
225 SFG with MitoTracker by live microscopy (**Fig. 3A**).

226 To determine the essentiality of DTC and YHM2 in *P. falciparum*, we attempted to delete
227 the genes individually in the parental NF54^{attB} line (**Fig. S2A**). Parasites lacking DTC or YHM2 were
228 confirmed by PCR (**Fig. 3B-C**, **Fig. S6**). Next, we used the same CRISPR plasmids to sequentially
229 disrupt the coding regions of DTC and YHM2 in Δ2 parasites. As before, we split the transfected
230 parasite culture into selective media with and without acetate. Drug-resistant parasites were
231 obtained in both acetate-free and supplemented media. We verified DTC and YHM2 deletions in
232 clonal lines using diagnostic PCR as well as by whole genome sequencing (**Fig. S7**, **Fig. S8**). Growth

233 comparisons of the triple (Δ*Pf*MPC1/*Pf*MPC2/DTC or Δ3) and quadruple
234 (Δ*Pf*MPC1/*Pf*MPC2/DTC/YHM2 or Δ4) mutants with parental parasites revealed only moderate
235 differences in replication rates (**Fig. 3D-E**). These results indicate that DTC and YHM2 are both
236 dispensable in ABS parasites and their absence does not confer large fitness costs to parasites.

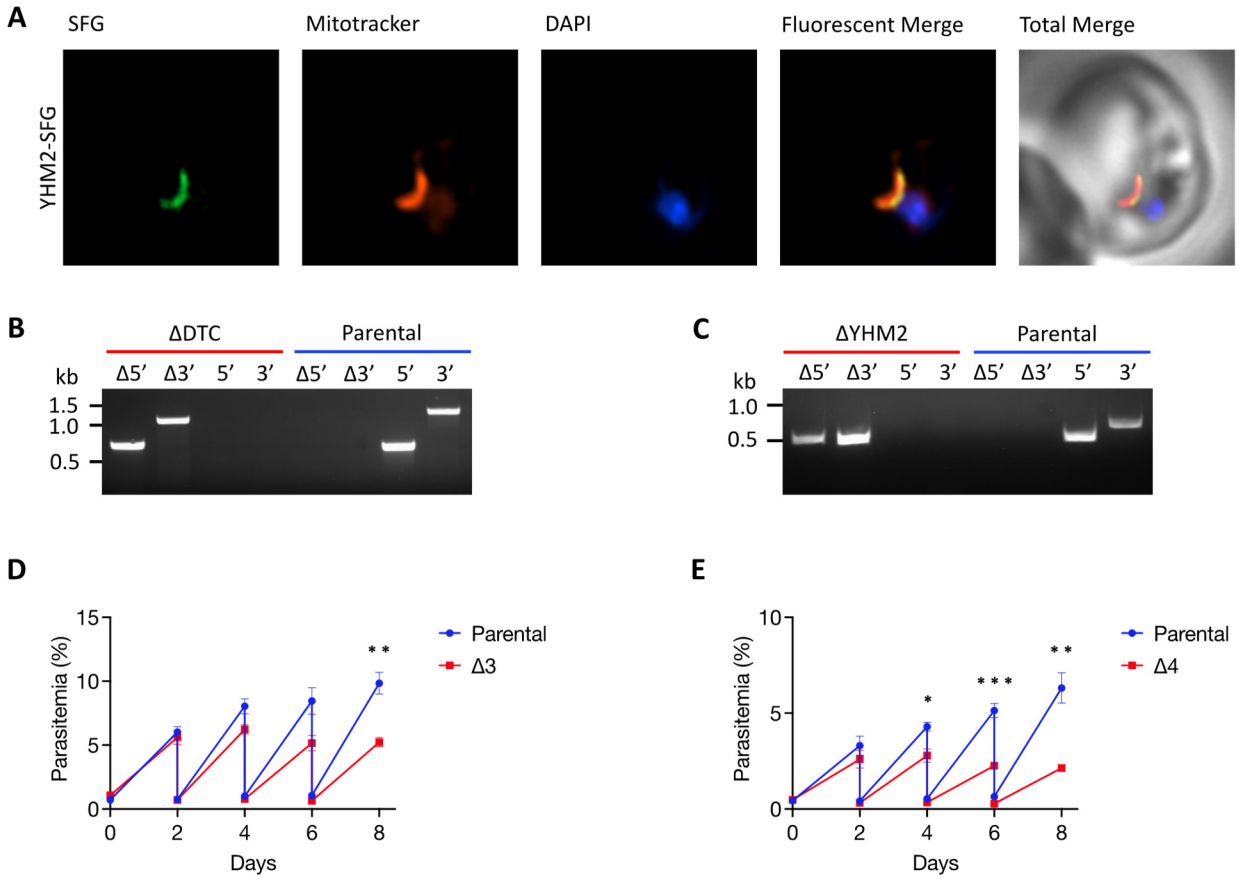

237

238 **Fig. 3. Multiple transporters are dispensable in ABS parasites.** (A) Representative immunofluorescence
239 microscopy images of YHM2-SFG parasites show that YHM2-SFG (green) colocalizes with MitoTracker
240 (red) [Mander's coefficient M1 (green in red) = 0.97, SD = 0.026, n = 16]. Images represent fields that are
241 10 μm long by 10 μm wide. Gene deletion of (B) DTC and (C) YHM2 in NF54^{attB} (parental) parasites was
242 confirmed by PCR amplification (Δ5′ and Δ3′ products). Intact gene loci (5′ and 3′ products) were detected
243 only in the parental (blue) and not in the mutant lines (red). Growth of parental, (D) Δ3, and (E) Δ4
244 parasites was compared by measuring their initial and final parasitemia over the 48-h developmental cycle
245 within red blood cells. The average fold change in parasitemia was calculated from the ratio of these
246 values to provide a measure of fitness. The data are from eight biological experiments with quadruplicate
247 samples. Error bars represent standard deviations from the mean. Statistics: Unpaired t-test using Prism

248 10 [GraphPad Software, Inc]; ns – not significant. Note: The growth data for the Δ3 line was collected
249 alongside Δ2, so the control parental data shown in Fig. 3D is identical to that in Fig. 1D.
250
251 **DTC and YHM2 transport α-ketoglutarate**
252 Although DTC and YHM2 are dispensable in ABS parasites, their absence could still affect
253 carbon import into the mitochondrion. To determine if the deletion of these genes in the Δ2
254 background confers an additive decrease in glucose carbon incorporation into acetyl-CoA, we
255 incubated Δ3, Δ4 and parental parasites in growth media containing $^{13}C_6$-glucose. As expected,
256 we observed a significant loss of two-carbon label (M+2) in acetyl-CoA and N-acetyl-glutamate
257 (**Fig. S9B-C**) in Δ3 and Δ4 mutants when compared with parental parasites. However, this
258 reduction was similar to what we observed with the Δ2 parasites (**Fig. 2C-D**). This suggests that
259 DTC and YHM2 do not play a major role in importing glucose carbon into the mitochondrion. As
260 observed with the double mutant, some two- and five-carbon label was still being incorporated
261 into citrate in Δ3 and Δ4 parasites (**Fig. S9D**).
262 The *P. falciparum* DTC protein has been shown to mediate efficient counter-transport of
263 α-ketoglutarate and other carboxylates *in vitro* (Nozawa et al., 2011). While the substrate
264 specificity of YHM2 has not been determined in malaria parasites, its homolog in yeast is a
265 citrate/α-ketoglutarate antiporter (Castegna et al., 2010). To test if *P. falciparum* DTC and YHM2
266 import glutamine carbon as α-ketoglutarate to feed the TCA cycle, we supplemented the growth
267 media of Δ3, Δ4, and parental parasites with $^{13}C_5$-glutamine. N-acetyl-glutamate and α-
268 ketoglutarate were fully labeled with $^{13}C_5$-glutamine carbon to a similar extent in all parasite lines
269 (**Fig. S9C**, **Fig. 4A-B**). On the other hand, we observed a substantial reduction in $^{13}C_5$-glutamine-
270 labeled succinate, fumarate, and malate in Δ3 parasites, and this defect was even more
271 pronounced in Δ4 parasites (**Fig. 4C-E**). Taken together, these results suggest that DTC and YHM2
272 are both responsible for the transport of α-ketoglutarate from the cytosol into the
273 mitochondrion.
274 Interestingly, succinate was found to contain three labeled carbons from glucose (M+3)
275 in Δ3 and Δ4 parasites but not in the parental or Δ2 lines (**Fig. 4C**, **Fig. S4B**). This M+3 succinate is
276 likely derived from an anaplerotic pathway in the cytosol that produces M+3 oxaloacetate from
277 the glycolytic intermediate phosphoenolpyruvate (Cobbold et al., 2013; MacRae et al., 2013;

278 Storm et al., 2014). Oxaloacetate can be converted into malate or aspartate in the cytoplasm,
279 with the latter generating fumarate during purine salvage (**Fig. 4A**) (Bulusu et al., 2011; Storm et
280 al., 2014). Anaplerotic glucose carbon may enter the TCA cycle as malate or fumarate. We
281 speculate that the reduced level of α-ketoglutarate in the mitochondria of Δ3 and Δ4 parasites
282 leads to a reversal in the direction of TCA cycle reactions downstream of KDH, with malate
283 successively converted to fumarate and succinate by fumarate hydratase and succinate
284 dehydrogenase, respectively. The end result is an accumulation of M+3 succinate in the Δ3 and
285 Δ4 parasite lines (**Fig. 4A**).

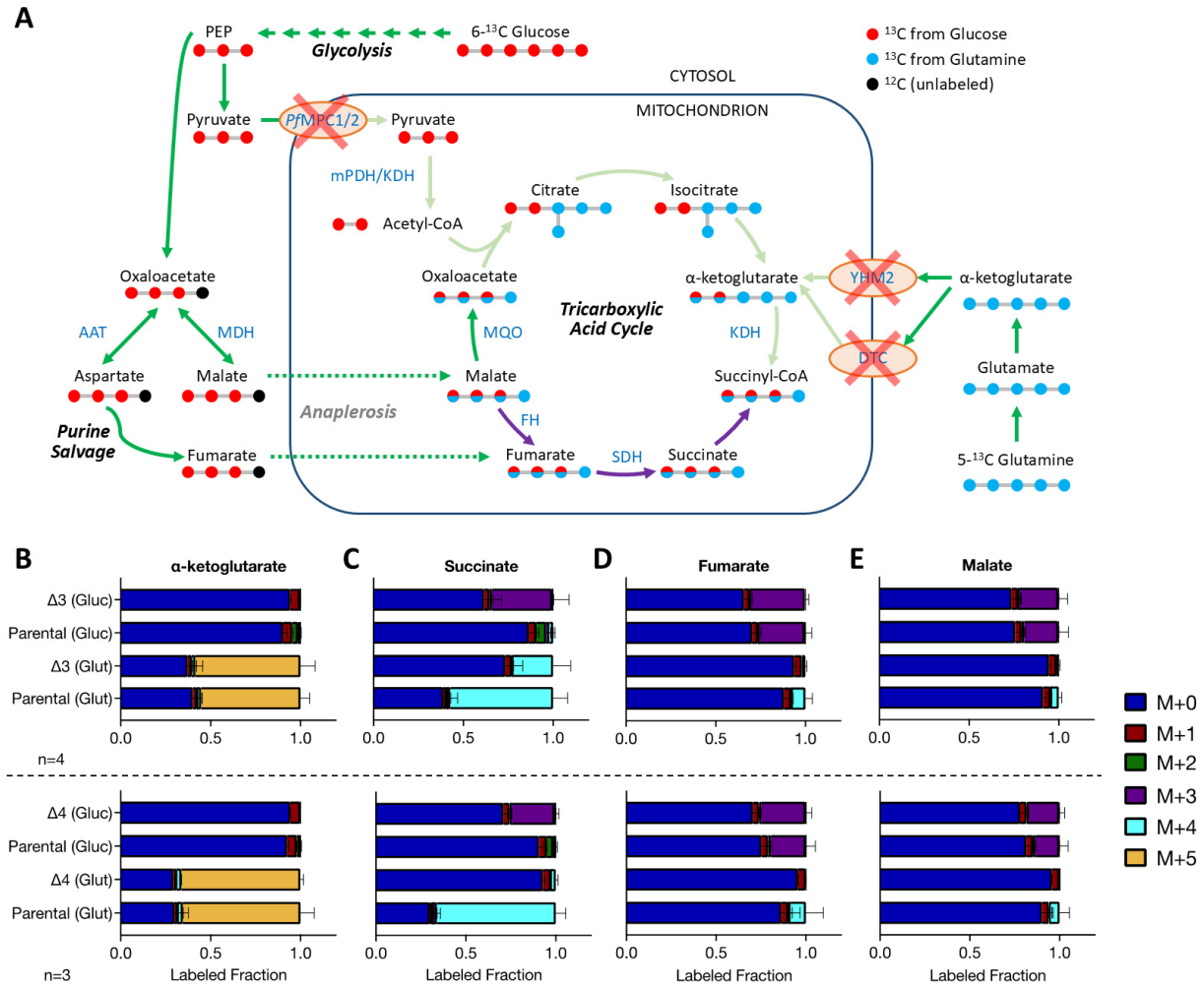

286

287 **Fig. 4. DTC and YHM2 control glutamine carbon incorporation into TCA cycle metabolites.** (A) Schematic
288 depicting the labeling pattern of mitochondrial metabolites in Δ4 parasites after short-term incubation
289 with uniformly labeled ^{13}C-glucose (solid red circles) or ^{13}C-glutamine (solid blue circles). Black circles

290 represent unlabeled atoms. Circles colored with both red and blue denote carbons that may be derived
291 from either $^{13}C_6$-glucose or $^{13}C_5$-glutamine, respectively. Arrows represent enzymatic reactions and are
292 colored based on the known flow (dark green), reduced flow (light green), predicted flow (dotted green)
293 or reverse flow (purple) of carbon atoms. Abbreviations: PEP – phosphoenolpyruvate; AAT – aspartate
294 aminotransferase; MDH – malate dehydrogenase; mPDH – mitochondrial pyruvate dehydrogenase; KDH
295 – α-ketoglutarate dehydrogenase; SDH – succinate dehydrogenase; FH – fumarate dehydrogenase; MQO
296 – malate-quinone oxidoreductase. (B-E) Fraction of isotopically labeled metabolites when parental, Δ3 or
297 Δ4 parasites are incubated with labeled glucose (Gluc) or glutamine (Glut). Color coding denotes the mass
298 (M) of the parent compound plus the mass shift from the incorporation of heavy carbon isotope (^{13}C).
299 Labeling data are expressed as the fraction of the total metabolite pool observed in 'n' independent
300 experiments. Error bars represent the standard deviations from the mean.
301
302 **Glucose limitation does not exacerbate growth defect of parasites lacking multiple carboxylate**
303 **transporters**
304 Despite the observed perturbations in central carbon metabolism, we did not see a large
305 fitness loss in the transporter mutants (**Fig. 1D**, **Fig. 3D-E**). We wondered if this was an artifact of
306 culturing parasites in medium with roughly twice the glucose concentration (11 mM) compared
307 to that found in human blood (4.0 – 6.5 mM). We therefore compared the growth of Δ4 and
308 parental parasites in regular culture medium (11 mM glucose) and low glucose (3.67 mM glucose)
309 medium over an 8-day period, with media replenishment every other day. While glucose levels
310 did not alter growth kinetics during the first cycle, both parasite lines exhibited similarly reduced
311 multiplication rates over the next three cycles in low glucose medium (**Fig. 5**). We therefore
312 conclude that the high levels of glucose in regular culture medium are not masking fitness defects
313 in Δ4 parasites.
314

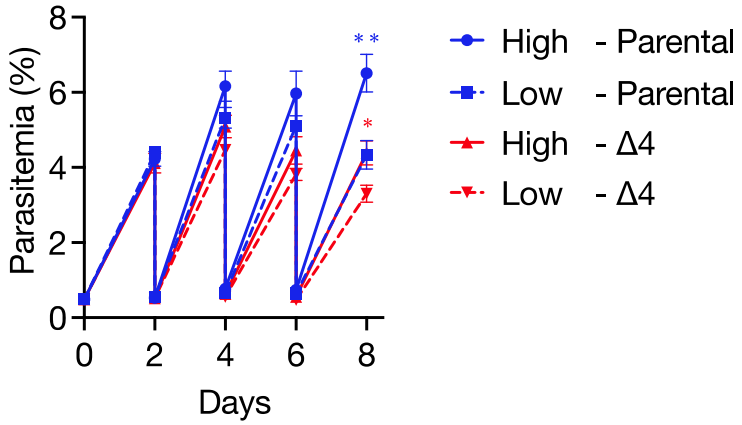

Fig. 5. Carboxylate transporter-deficient parasites do not exhibit heightened sensitivity to low glucose conditions. Growth of parental and Δ4 parasites in low (3.67 mM) and high (11 mM) glucose media was monitored by flow cytometry over an 8-day period. Cultures were seeded at 0.5% parasitemia on day 0 and diluted 1:8 every other day. Two biological experiments were conducted in quadruplicate. Error bars represent the standard deviations from the mean. Statistics: Two-way ANOVA using Prism 10 [Graphpad Software, Inc], with Šídák's multiple comparison test; *, $p \leq 0.05$; **, $p \leq 0.01$.

Deletion of mitochondrial transporters does not alter parasite responsiveness to dihydroartemisinin

The mitochondrion of the malaria parasite is a key target of artemisinins. These drugs exert their antimalarial effects in part by inducing rapid mitochondrial membrane depolarization (Peatey et al., 2015; Wang et al., 2010). Arteminisin-resistant parasites have been found to exhibit altered mitochondrial energy metabolism, with a broad upregulation of genes linked to mitochondrial transport and pathways related to pyruvate, glutamate, and acetyl-CoA metabolism (Chen et al., 2014; Mok et al., 2021; Yu et al., 2023). In particular, transcription of the YHM2 transporter gene is upregulated in several clinically resistant isolates; however, whether this single-handedly alters responsiveness to artemisinin has not been established (Bonive-Boscan et al., 2023; Tripathi et al., 2023; Zhang et al., 2022; Zhu et al., 2022).

We utilized the ΔYHM2 and the dual copy parasite lines to determine the impact of increased gene dosage of YHM2 versus no expression on sensitivity to dihydroartemisinin (DHA). Employing standard 72-h proliferation assays, we found that the two transgenic strains and the NF54^{attB} parent had comparable IC_{50} values for DHA (Parental – 1.9 nM; YHM2-SFG – 1.8 nM;

339 ΔYHM2 – 2.5 nM) (**Fig. 6A-B**). Since the Δ4 transporter mutant exhibits altered pyruvate and
340 glutamate metabolism, we also assessed its sensitivity to DHA. We did not observe a notable shift
341 in the IC_{50} value (Parental – 1.7 nM; Δ4 – 1.4 nM) (**Fig. 6C**).
342 Artemisinin resistance is characterized by delayed parasite clearance in patients and
343 increased survival of early ring stage parasites *in vitro* (Amaratunga et al., 2012; Dondorp et al.,
344 2009; Witkowski et al., 2010). The latter can be assessed through a ring-stage survival assay (RSA)
345 in which 0-3 h rings are exposed to 650 nM DHA for 6 h and their recovery is measured after 66
346 h (Witkowski et al., 2013). We conducted parallel RSAs for the mutant and parent parasites and
347 found that neither YHM2 overexpression nor deletion of one or multiple mitochondrial
348 transporters influenced the ring-stage survival percentage (**Fig. 6D**). Therefore, our data suggest
349 that changes in mitochondrial transporter expression alone do not alter the susceptibility of *P.*
350 *falciparum* to DHA.
351

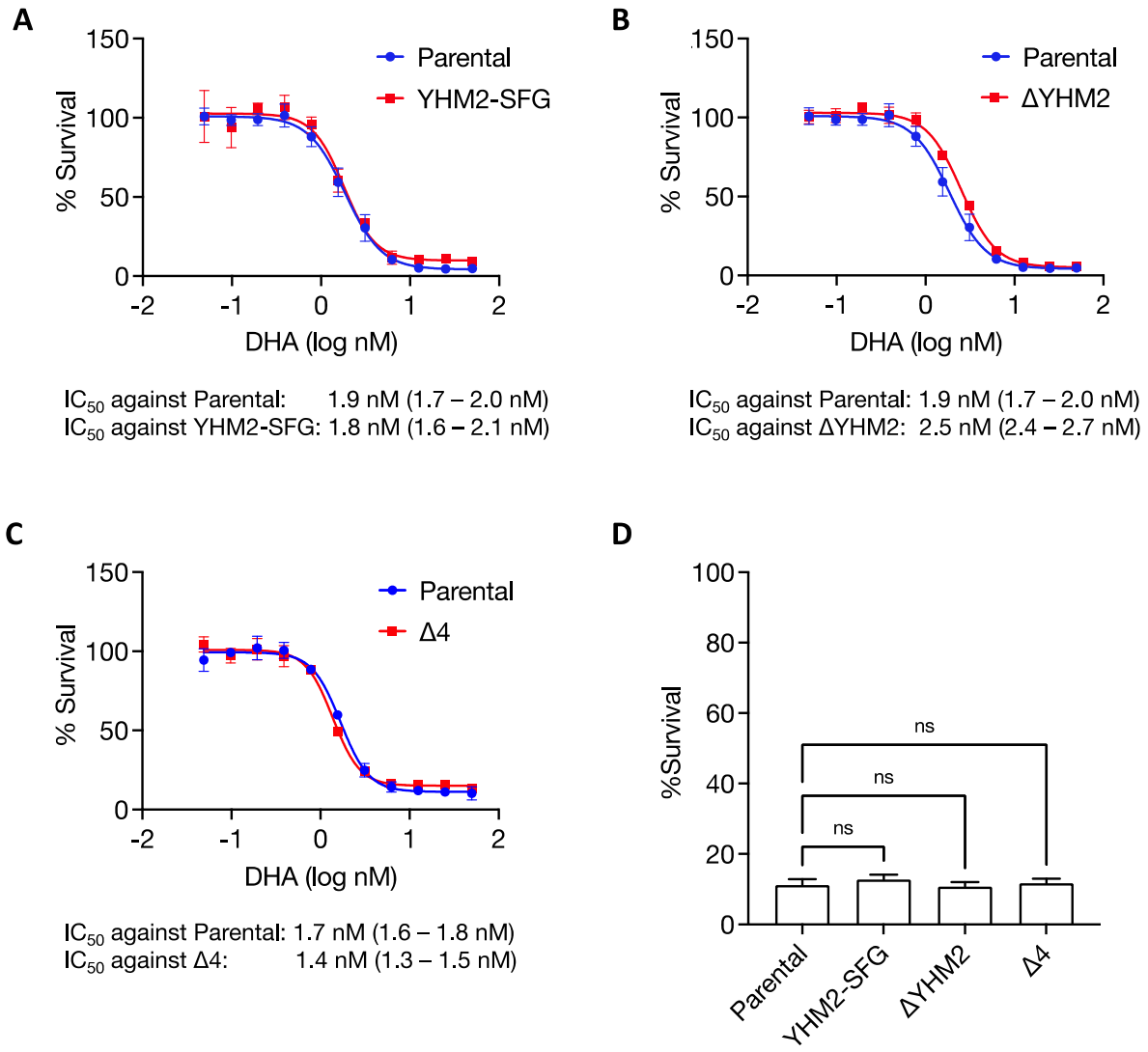

Fig. 6. Mitochondrial transporter mutants do not show altered susceptibility to dihydroartemisinin (DHA). Parasites that (A) express a second copy of YHM2 under the constitutively active Cam/HOP promoter, (B) contain a YHM2 gene deletion, or (C) contain deletions in *Pf*MPC1, *Pf*MPC2, DTC and YHM2 genes, were exposed to various concentrations of dihydroartemisinin (DHA) for 72 h followed by measurement of parasitemia via flow cytometry. Parental parasites were employed as control. Two independent biological experiments with quadruplicate samples were conducted. Error bars represent the standard deviation from the mean. The parental data are identical in Fig. 6A and 6B since these experiments were conducted concurrently. The calculated IC_{50} values for DHA (with 95% confidence intervals in brackets) are listed below the graphs. C) Survival percentages from a ring-stage assay for parental, YHM2-SFG, ΔYHM2, and Δ4 parasites are depicted. Two independent biological experiments

363 were conducted with quadruplicate samples and parasitemia was measured by flow cytometry at 66 h.
364 Error bars represent the standard deviations from the mean. Statistics: IC_{50} values were obtained using a
365 nonlinear variable slope four-parameter regression curve fitting model in Prism 10 [GraphPad Software
366 Inc.]. One-way ANOVA with Dunnett's correction in Prism 10 was used to compare differences between
367 RSA survival percentages; ns – not significant.
368
369 **DISCUSSION:**

370 Acetyl-CoA is a universally required metabolite that orchestrates numerous cellular
371 processes mainly by donating its two-carbon acetyl group to recipient molecules (Shi and Tu,
372 2015). Because it is membrane-impermeable, distinct pools of acetyl-CoA are typically
373 maintained by enzymes in various subcellular compartments. In the mitochondria of most
374 eukaryotes, acetyl-CoA is derived from glucose, fatty acid, and branched-chain amino acid
375 catabolism, and it undergoes complete oxidation through the TCA cycle to generate ATP and CO_2.
376 Cytosolic acetyl-CoA, which is required for lipid and isoprenoid synthesis, can be sourced in at
377 least two ways: from the export and cleavage of mitochondrial citrate by ATP-citrate lyase, or
378 from acetate by an acetyl-CoA synthetase (ACS). Acetyl-CoA can enter the nucleus through the
379 nuclear pore or can be additionally generated by a resident ACS to regulate gene expression via
380 acetylation of histones and transcription factors. The *P. falciparum* genome appears to encode
381 some, but not all, of the enzymes responsible for acetyl-CoA production. During asexual blood
382 stage development, the mitochondrion serves as the principal source of acetyl-CoA for the entire
383 parasite (Nair et al., 2023). The pathways for BCAA degradation and fatty acid oxidation are either
384 missing or incomplete, which leads us to surmise that glycolytic pyruvate is the primary substrate
385 for acetyl-CoA synthesis in the mitochondrion (Cobbold et al., 2013; Gardner et al., 2002; MacRae
386 et al., 2013; van Dooren et al., 2006). Indeed, inactivation of mPDH and KDH, the enzymes
387 required for the conversion of pyruvate to acetyl-CoA, is lethal for parasites (Nair et al., 2023).
388 Given the critical role of pyruvate in the mitochondrion, this study aimed to determine how
389 pyruvate is mobilized from the cytoplasm into the organelle in malaria parasites.

390 We targeted two putative mitochondrial pyruvate carrier proteins – *Pf*MPC1 and *Pf*MPC2
391 –for genetic and metabolic studies in *P. falciparum*. While gene deletion of one or both proteins
392 surprisingly did not strongly affect parasite viability in red blood cells, our isotopic labeling

393 analyses revealed that the ^{13}C label from glucose was considerably diminished in acetyl-CoA.
394 However, this reduction was not as severe as seen previously in the mPDH/KDH double-deletion
395 mutant, which suggested that one or more redundant mechanisms facilitate glucose carbon
396 entry into the mitochondrion (Nair et al., 2023). To determine if other mitochondrial carriers can
397 transport pyruvate, we turned our attention to two carboxylate carrier proteins, DTC and YHM2.
398 Single and combinatorial deletion mutants were successfully obtained with modest fitness costs.
399 Treatment of Δ3 (Δ*Pf*MPC1/*Pf*MPC2/DTC) and Δ4 (ΔMPC1/*Pf*MPC2/DTC/YHM2) mutants with
400 $^{13}C_6$-glucose demonstrated that the absence of DTC and YHM2 does not noticeably affect the
401 levels of pyruvate-derived acetyl-CoA. Taken together, these results establish that *Pf*MPCs are
402 the primary mitochondrial pyruvate carriers, but in their absence, an alternative path exists for
403 some cytosolic pyruvate to enter the mitochondrion.

404 Although additional details of acetyl-CoA synthesis in the *P. falciparum* mitochondrion
405 remain to be established, we were able to gain new insights into how another major carbon
406 source, α-ketoglutarate, is imported into the organelle. Our $^{13}C_5$-glutamine labeling data show
407 that DTC plays a key role in facilitating glutamine carbon entry into the TCA cycle as α-
408 ketoglutarate. In *P. falciparum*, glutamine is initially converted by glutamine synthetase to
409 glutamate, which can then be converted to α-ketoglutarate in the cytosol by aspartate
410 aminotransferase or by glutamate dehydrogenases (Storm et al., 2011). A putative GABA
411 transaminase is speculated to convert glutamate to α-ketoglutarate in the mitochondrion, but
412 our results indicate that the bulk of glutamine carbon reaches the organelle as α-ketoglutarate,
413 not as glutamate (Cobbold and McConville, 2014). This is evidenced by the observation that DTC
414 deletion did not impact glutamine incorporation into α-ketoglutarate, but it affected the labeling
415 of other TCA cycle metabolites. Additional deletion of YHM2 exacerbated this metabolic
416 phenotype, consistent with both transporters importing α-ketoglutarate and conversion of
417 glutamine to α-ketoglutarate occurring prior to mitochondrial import.

418 The anaplerotic influx of glucose carbon into the TCA cycle has been attributed to DTC,
419 which can transport oxaloacetate, malate and to a lesser extent, fumarate *in vitro* (Ke et al., 2015;
420 Nozawa et al., 2011). Interestingly, DTC deletion did not block anaplerotic M+3 carbon
421 assimilation into TCA cycle intermediates. On the contrary, we noted a large increase in M+3

422 succinate species when compared with parental parasites. We attribute this buildup to a reversal
423 in the flow of glucose carbon from M+3 malate/fumarate in response to low levels of α-
424 ketoglutarate in the mitochondrion. So, if DTC is not the relevant transporter, how does
425 anaplerotic glucose carbon get into the mitochondrion, and in what form? A previous study
426 indicated that M+3 oxaloacetate does not enter the organelle; the unknown mitochondrial
427 carrier must therefore import anaplerotic fumarate or malate (Ke et al., 2015). If the carrier
428 exhibits broad specificity for carboxylates, it might also serve as the redundant pyruvate
429 transporter.

430 Although YHM2 is annotated as a citrate/α-ketoglutarate antiporter, it is difficult to
431 determine whether the deletion of YHM2 impacts citrate levels in the mitochondrion and the
432 cytoplasm, since our data reflect metabolite levels in the infected red blood cell as a whole. Even
433 if YHM2 exports citrate from the mitochondrion, the fate of citrate in the cytoplasm is uncertain
434 since malaria parasites do not appear to contain an ATP-citrate lyase to transform citrate into
435 acetyl-CoA (Gardner et al., 2002). The yeast YHM2 homolog supports biosynthetic reactions and
436 antioxidant defense by coupling citrate/α-ketoglutarate transport to NADPH generation
437 (Castegna et al., 2010). While it is unclear if NADPH can be formed from citrate interconversion
438 in the cytoplasm of *P. falciparum*, YHM2 has been recently linked to the artemisinin resistance
439 phenotype, with such parasites demonstrating increased tolerance to drug-induced oxidative
440 damage (Rocamora et al., 2018). The YHM2 gene is one of several genes associated with
441 mitochondrial energy metabolism that are upregulated in resistant clinical isolates (Tripathi et
442 al., 2023; Zhu et al., 2022). We found that deleting or expressing a second copy of YHM2 did not
443 alter parasite susceptibility to DHA, indicating that YHM2 is not sufficient to significantly alter
444 artemisinin resistance.

445 The metabolite data collected from our series of combinatorial deletion mutants allowed
446 us to propose substrate specificities for several mitochondrial carriers. Our results also
447 underscore the high degree of functional redundancy and plasticity in *P. falciparum* parasites, as
448 evidenced by their ability to survive the loss of four carrier proteins. The gene deletion results
449 presented in this study are not entirely concordant with a forward genetic screen for essentiality
450 in *P. falciparum*, in which *Pf*MPC1, *Pf*MPC2 and DTC were all assigned low mutability scores

451 (**Table 1**) (Zhang et al., 2018). However, the relatively small sizes of the coding sequences of these
452 genes (*Pf*MPC1: 318 bp, *Pf*MPC2: 387 bp, DTC: 954 bp) decrease the predictive capability of the
453 screen. On the other hand, YHM2 was identified as dispensable in both *P. falciparum* and *P.*
454 *berghei* screens (Schwach et al., 2015; Zhang et al., 2018). Therefore, targeted gene deletion
455 studies remain important to determine the functional role of genes expressed during the asexual
456 blood stage.

Gene ID (PF3D7_)	Gene name	Essentiality in asexual blood-stage *Plasmodium*				Mitochondrial Localization	
		P. falciparum (a)		*P. berghei* (b)	*P. falciparum* (this study)	MitoProtII (c)**	PlasmoMitoCarta (d)**
		MFS*	MIS*				
1340800	Mitochondrial pyruvate carrier 1 (*Pf*MPC1)	-3.235	0.119	Not studied	Dispensable	0.8878	5.97197
1470400	Mitochondrial pyruvate carrier 2 (*Pf*MPC2)	-2.167	0.331	Not studied	Dispensable	0.6315	6.87333
0823900	Di/tricarboxylic acid carrier (DTC)	-2.799	0.162	Not studied	Dispensable	0.2626	3.54392
1223800	Citrate/α-ketoglutarate transporter (YHM2)	-0.31	1	Dispensable	Dispensable	0.1695	1.31981

457
458 **Table 1. Essentiality of mitochondrial transporter genes from forward and reverse genetic approaches.**
459 a – Zhang et al., 2018; b – Schwach et al., 2015; c – Claros and Vincens, 1996; d – Esveld et al., 2021.
460 * The *P. falciparum* genome-wide screen for essential genes (Zhang et al., 2018) utilized MFS (mutagenesis
461 fitness score) and MIS (mutagenesis index score) ranging from 0 to 1 to predict gene mutability. Low MFS
462 and MIS scores indicate gene essentiality.
463 ** MitoProtII scores (ranging from 0 to 1) and PlasmoMitoCarta scores (ranging from -17.2747 to 12.486)
464 predict mitochondrial localization of *Plasmodium* proteins. Proteins with high MitoProtII scores and high
465 PlasmoMitoCarta scores have a higher probability of localizing to the mitochondrion.
466
467 In summary, our study demonstrated that pyruvate is imported into the mitochondrion
468 of *P. falciparum* parasites via *Pf*MPC1 and *Pf*MPC2 and at least one additional path. We also found
469 that α-ketoglutarate is transported into the mitochondrion by DTC and YHM2 to feed the TCA
470 cycle. It remains to be determined how acetyl-CoA is exported from the mitochondrion for
471 utilization in other intracellular compartments. The importance of acetyl-CoA metabolism in
472 malaria parasites warrants further experimentation to identify and characterize novel
473 mitochondrial carriers that support the synthesis and utilization of this critical metabolite.
474
475 **METHODS:**

476 **Parasite culture**

477 *P. falciparum* NF54^{attB} parasites were cultured in red blood cells (RBCs) at 2% hematocrit
478 in complete medium with AlbuMAX II (CMA). CMA is prepared from RPMI-1640 medium with L-
479 glutamine (USBiological Life Sciences, R8999) and is supplemented with 20 mM HEPES, 0.2%
480 sodium bicarbonate, 12.5 µg/mL hypoxanthine, 5 g/L AlbuMAX II (ThermoFisher Scientific,
481 11021037) and 25 µg/mL gentamicin. Parasite cultures were maintained at 37°C in a gas mixture
482 containing 94% N_2, 3% O_2 and 3% CO_2.

483

484 **Plasmid construction**

485 Localization constructs were derived from the previously published p15-EcDPCK-mCherry
486 plasmid (Swift et al., 2021). The mCherry tag was removed by digesting the plasmid with BsiWI
487 and AflII, and replaced with an SFG sequence that was amplified using primers listed in **Table S1**
488 and the p15-Mev-aSFG plasmid as template (Swift et al., 2020b). The SFG amplicon was digested
489 with BsiWI and AflII and ligated with the cut p15-EcDPCK plasmid using T4 DNA Ligase (NEB,
490 M0202). The EcDPCK gene was replaced with *Pf*MPC1, *Pf*MPC2, YHM2 or DTC coding sequences
491 by digesting the plasmid with AvrII and BsiWI. The coding sequences were amplified from *P.*
492 *falciparum* NF54^{attB} genomic DNA (mRNA for *Pf*MPC1 and *Pf*MPC2 to exclude introns) with
493 primers included in **Table S1**. The amplicons were digested with BsiWI and AflII and ligated into
494 the digested p15-SFG plasmid.

495 Gene deletion constructs for *Pf*MPC1, *Pf*MPC2, DTC and YHM2 were generated using
496 several versions of pRSng repair plasmids with different drug resistance cassettes (Rajaram et al.,
497 2022; Swift et al., 2020b). Homology arms 1 (HA1) and 2 (HA2) for the genes were amplified using
498 primers listed in **Table S1**. The HA1 sequence was inserted into the NotI site and HA2 into the
499 NgoMIV site of the repair plasmid. For individual knockouts of the *Pf*MPC genes, we used the
500 original pRSng plasmid which contains a hDHFR (human dihydrofolate reductase) resistance
501 cassette that confers resistance to the drug WR99210 (Swift et al., 2020b). For deletion of
502 *Pf*MPC1 in the Δ*Pf*MPC2 background, hDHFR was replaced with blasticidin deaminase (BSD) to
503 generate a *Pf*MPC1-pRSngBD plasmid. Homology arms for DTC were cloned into a pRSng-Neo
504 plasmid containing a neomycin cassette, providing resistance to G418 (Rajaram et al., 2022).

505 Finally, homology arms for YHM2 were cloned into a pRSng-Mev plasmid which contains a
506 mevalonate cassette that provides resistance to fosmidomycin. To create the pRSng-Mev
507 plasmid, the pRSng and p15-Mev-aSFG plasmids were digested with BamHI and HindIII to replace
508 the hDHFR cassette in pRSng with the Mev-aSFG cassette from p15-Mev-aSFG using ligation
509 (Swift et al., 2020b).

510 To generate plasmids with guide RNA sequences that target *Pf*MPC1, *Pf*MPC2, DTC and
511 YHM2 for gene deletion, the pCasG-LacZ vector was digested with the type IIS restriction enzyme
512 BsaI (Rajaram et al., 2020). Guide RNAs were synthesized as oligonucleotides (**Table S1**),
513 annealed, and inserted into the cut plasmid. Unless specified, plasmid construction relied on
514 ligation-independent cloning with In-Fusion (Takara, 638944). Restriction enzymes were sourced
515 from New England Biolabs.

516

517 **Parasite transfections**

518 To determine the subcellular localization of *P. falciparum* transporter proteins, 350 µL
519 volumes of RBCs were electroporated using the GenePulser XCell system (Bio-Rad) with: 50 µg of
520 the pINT plasmid (Nkrumah et al., 2006) that expresses the Bxb1 integrase, and 65 µg of the p15-
521 SFG plasmid expressing either *Pf*MPC1, *Pf*MPC2, DTC or YHM2 fused to a C-terminal SFG tag. The
522 electroporated RBCs were mixed with 1 mL of NF54^{attB} parasite culture at 2-3% parasitemia and
523 maintained in 10 mL of CMA for 2 days. They were then transferred to selective media containing
524 2.5 nM WR99210 for 7 days. The cultures were then returned to CMA until blood smears turned
525 parasite-positive, whereupon WR99210 was added back to the medium.

526 To generate deletion strains, 350 µL volumes of RBCs were electroporated with 65 µg
527 each of the repair plasmid and the appropriate pCasG-gRNA plasmid. The electroporated RBCs
528 were mixed with 1 mL of parasite culture at 2-3% parasitemia and maintained in 10 mL of CMA
529 for 2 days. They were then transferred to selective media containing 1.5 µM DSM1 and either 2.5
530 nM WR99210 (for individual deletions of *Pf*MPC1 and *Pf*MPC2), 0.5 mg/mL G418 (for DTC
531 knockout), or 25 µM fosmidomycin plus 50 µM mevalonolactone (for YHM2 knockout) for 7 days.
532 Cultures were then switched to CMA until parasites reappeared, after which they were
533 transferred to CMA containing WR99210 (Δ*Pf*MPC1 and Δ*Pf*MPC2) or G418 (ΔDTC). To delete

534 *Pf*MPC1 in the Δ*Pf*MPC2 line, RBCs were electroporated with the pRSngBD-*Pf*MPC1 plasmid and
535 the same pCasG-gRNA plasmid employed earlier. Two days post transfection, the culture was
536 selected with 2.5 µg/mL blasticidin for 7 days. Culture media then was replaced with CMA, and
537 maintained as such until parasite reappearance, at which point blasticidin was reintroduced into
538 the media.

539 All transgenic parasite lines were cloned by limiting dilution. Drugs were acquired from
540 the following vendors: DSM1 – Calbiochem (CAS 92872-51-0); WR99210 – Jacobus
541 Pharmaceutical Company, Inc.; Blasticidin – Corning (30-100-RB); G418 – Corning (61-234-RG),
542 Fosmidomycin – ThermoFisher Scientific (FR-31564), Mevalonolactone – Sigma-Aldrich (M4667).
543

544 **Genotyping PCR**

545 Three µL volumes of parasite culture were used in 25 µL PCR reactions with Phusion High-
546 Fidelity DNA polymerase (NEB, M0530). Primer pairs and anticipated sizes of PCR products are
547 indicated in **Fig. S1** and **Fig. S2**. Primer sequences can be found in **Table S1**.
548

549 **Growth assays**

550 The growth rates of gene knockout lines were compared against the parental line to
551 determine if gene deletions imparted fitness costs. Parasites were used to seed 200 µL culture
552 volumes/well in a 96-well plate (ThermoFisher Scientific, 267427) at a 0.5% starting parasitemia
553 and 2% hematocrit. The plates were incubated in chambers gassed with 94% N_2, 3% O_2, 3% CO_2
554 at 37°C. After 48 h (the duration of an asexual intraerythrocytic developmental cycle), final
555 parasitemia was determined by flow cytometry. This process was repeated over at least four
556 growth cycles, with an eight-fold dilution of cultures every 48 h to prevent overgrowth. Samples
557 were prepared for flow cytometry as described previously (Swift et al., 2020b). Briefly, parasites
558 were diluted 1:5 in PBS and stored in a 96-well plate at 4 °C until analysis by flow cytometry.
559 Parasites were stained by transferring 10 µL of the 1:5 dilutions to a 96-well plate containing 100
560 µL of 1x SYBR Green (Invitrogen, S7563) in PBS, and incubated for 30 minutes in the dark while
561 shaking. Post-incubation, 150 µL of PBS was added to each well to dilute unbound SYBR Green
562 dye. Stained cells were analyzed with an Attune NxT Flow Cytometer (ThermoFisher Scientific) at

563 a running speed of 25 µL/minute to acquire 10,000 events. Experiments were conducted with
564 quadruplicate samples.
565
566 ***P. falciparum* purification, isotopic labeling, and metabolomics analysis**
567 Heparin-synchronized NF54^{attB} parental (Adjalley et al., 2011) and associated knockout
568 strains of *P. falciparum* parasites were cultured in standard conditions. At approximately 24-30
569 hours post invasion, healthy trophozoite stage parasites were purified via magnet activated cell
570 sorting using a SuperMACS™ II Separator (Miltenyi Biotec, 130-044-104) and a D column (Miltenyi
571 Biotec, 130-041-201). The samples of ~95-100% pure trophozoite-infected erythrocytes were
572 plated at 0.2% hematocrit in standard culture media and incubated for a one-hour recovery
573 period. After recovery, the parasites were pelleted, the standard culture media supernatant was
574 discarded, and parasites were resuspended in complete media made with either glucose-dropout
575 (Gibco, 11879-020) or glutamine-dropout (Gibco, 21870-076) base RPMI-1640 supplemented
576 with 25mM HEPES pH 7.4 (Millipore Sigma, H4034), 2 g/L sodium bicarbonate (Fisher Scientific,
577 BP328), 10 mg/L hypoxanthine (Fisher Scientific, AC122010250), 2.5 g/L AlbuMAX II (Thermo
578 Fisher Scientific, 11021029), 50 mg/L gentamicin sulfate (Bio Basic, GB0217). 11 mM $^{13}C_6$-glucose
579 (Cambridge Isotope Laboratories, CLM-1396-1) or 2 mM $^{13}C_5$-glutamine (Cambridge Isotope
580 Laboratories, CLM-1822-H) was added to respective dropout media. Parasites were cultured in
581 6-well culture plates at 1x10^8 cells/5 mL media in technical triplicate for a 2.5 hour labeling
582 period.
583 After pelleting and washing in ice cold PBS pH 7.4, the infected erythrocytes were then
584 resuspended in 1 mL of 90% HPLC-grade methanol with 0.5 µM [$^{13}C_4$,$^{15}N_1$] aspartate (Millipore
585 Sigma, 607835) as an internal control. Supernatants were dried under nitrogen gas flow and
586 stored at -70°C before being resuspended to 10^6 former cells/µL in HPLC-grade water with 1µM
587 chlorpropamide (Alfa Aesar, J64110) as an additional internal control for reverse phase UHPLC-
588 MS analysis on a Thermo Exactive Plus Orbitrap. For each sample, 10 µL were injected through a
589 XSelect HSS T3 2.5 µM C18 column (Waters, 186006151) and eluted using a 25 min gradient of
590 3% aqueous methanol, 15 mM acetic acid (Millipore Sigma, A6283), 10 mM tributylamine
591 (Millipore Sigma, 90781), 2.5 µM medronic acid ion pairing agent (Millipore Sigma, M9508) (A)

592 and 100% HPLC-grade methanol (B). Negative-ion mode, using a scan range of 85 to 1,000 *m/z*
593 and a resolution of 140,000 at *m/z* 200 was used for ion detection.
594 Resulting .raw files were converted to .mzML format and centroided using the MSConvert
595 software of the ProteoWizard package (Chambers et al., 2012). The .mzML files were then
596 aligned, peaks picked, and peaks annotated (including isotopic variants) with El-MAVEN (Agrawal
597 et al., 2019). The chlorpropamide internal standard intensity as well as pooled quality control
598 (QC) samples were used to evaluate technical reproducibility of ion detection across the run. EL-
599 MAVEN-called peaks were then manually curated based on the proximity to the standard
600 retention time in the targeted library, signal/blank ratio, and peak shape. Integrated areas of
601 acceptable peaks were exported from EL-MAVEN in a.csv file and further processing was
602 performed using Microsoft Excel.
603 Chlorpropamide standard abundance was used to correct the peak areas per metabolite
604 for instrument variation in ion detection during the run. Subsequently, the average blank signals
605 were subtracted (or substituted to avoid negative abundances), and metabolites were filtered
606 based on the relative standard deviation (RSD, Standard Deviation/Mean) of QC samples run
607 regularly throughout data collection and the metabolites were excluded from analysis if RSD >
608 30% (**Supplemental File 2**). Raw data for all metabolites are available at the NIH workbench under
609 submission Project ID: PR002196.
610
611 **Whole genome sequencing of clonal parasite lines**
612 Parasites used for genomic DNA (gDNA) extraction were grown to 8 - 10 % schizonts in a
613 50-mL culture at 2% hematocrit. Cells were isolated by centrifugation (400 g for 3 minutes) before
614 aspirating the supernatant and adding 50 mL of 0.1% saponin in PBS. Following 10 minutes of
615 lysis, parasites were isolated by centrifugation (1,500 g for 10 minutes) and washed twice with
616 50 mL of PBS. The gDNA was extracted using a Qiagen DNeasy Blood and Tissue kit (69504)
617 according to the provided protocol. Extracted gDNA was quantified using a Nanodrop
618 spectrophotometer or a Qubit 2.0 fluorometer. Sequencing libraries for Δ2 and Δ3 lines were
619 prepared with 1 µg of gDNA per sample using the TruSeq® DNA PCR-Free Low-Throughput Library
620 Prep Kit (Illumina, 20015962) according to the manufacturer's directions. The Δ2 and Δ3 libraries

621 were sequenced on a HiSeq2500 Illumina platform. The sequencing library for the Δ4 line was
622 prepared with 100 ng of gDNA using the Celero PCR Workflow and an Enzymatic Fragmentation
623 DNA Seq Kit (Tecan, 30238472). This library was sequenced on the iSeq 100 Illumina platform.
624 Genomic sequence data for the Δ2, Δ3 and Δ4 transgenic lines are available at the NCBI Sequence
625 Read Archive under submission BioProject PRJNA1181605.
626
627 **IC_{50} and ring-stage survival assays for DHA**
628 To perform dose-response experiments with DHA, late-stage parasites from the parental
629 $NF54^{attB}$, ΔYHM2, YHM2-SFG and Δ4 lines were magnetically sorted from mixed-stage cultures
630 using MACS LS columns (Miltenyi Biotech, 130-042-401). The purified parasites were diluted to
631 1% parasitemia in 1.5% hematocrit and incubated with serial dilutions of DHA resuspended in
632 DMSO to achieve a final DMSO concentration of 0.1%. After 72 h of incubation in standard
633 culturing conditions, parasitemia was measured by flow cytometry as described above.
634 For ring-stage survival assays, cultures were synchronized by magnetic column
635 enrichment of late-stage parasites over two consecutive ABS cycles. After a 3 h period for
636 reinvasion, parasites were treated with 5% sorbitol before initiation of the assay to remove any
637 late-stage parasites. The highly synchronized ring-stage parasites from $NF54^{attB}$, ΔYHM2, YHM2-
638 SFG and Δ4 lines were maintained for 6 hours in CMA containing 650 nM of DHA in 0.1% DMSO.
639 Simultaneously, parasites were incubated in CMA with 0.1% DMSO only to serve as controls.
640 Following the 6 h incubation, the cultures were washed three times in CMA to remove drug or
641 DMSO. The washed parasites were further cultured for 66 h before measurement of parasitemia
642 by flow cytometry. Survival rates for each parasite line were determined by calculating the
643 percentage of surviving DHA-treated parasites to DMSO-treated parasites.
644
645 **ACKNOWLEDGEMENTS**
646 This work was supported by NIH R01 AI168183 (awarded to S.T.P. and M.L.), the Johns
647 Hopkins Malaria Research Institute, and the Bloomberg Family Foundation. K.R. was supported
648 by the Johns Hopkins Discovery Award, G.R. was supported by a Penn State Eberly Research
649 Fellowship, and J.T.M. was supported by training grant T32 DK120509. M.L. was also supported

650 by the Eberly College of Science and the Huck Institutes of the Life Sciences at The Pennsylvania
651 State University. The authors would like to acknowledge the Huck Institutes' Metabolomics Core
652 Facility (RRID:SCR_023864) for maintenance of the Thermo Exactive Plus.

653 Adjalley, S.H., Johnston, G.L., Li, T., Eastman, R.T., Ekland, E.H., Eappen, A.G., Richman, A., Sim,
654 B.K.L., Lee, M.C.S., Hoffman, S.L., Fidock, D.A., 2011. Quantitative assessment of
655 Plasmodium falciparum sexual development reveals potent transmission-blocking
656 activity by methylene blue. Proc Natl Acad Sci U S A 108, E1214-1223.
657 https://doi.org/10.1073/pnas.1112037108
658 Adjalley, S.H., Lee, M.C.S., Fidock, D.A., 2010. A Method for Rapid Genetic Integration into
659 Plasmodium falciparum Utilizing Mycobacteriophage Bxb1 Integrase, in: Braman, J.
660 (Ed.), In Vitro Mutagenesis Protocols, Methods in Molecular Biology. Humana Press,
661 Totowa, NJ, pp. 87–100. https://doi.org/10.1007/978-1-60761-652-8_6
662 Agrawal, S., Kumar, S., Sehgal, R., George, S., Gupta, R., Poddar, S., Jha, A., Pathak, S., 2019. El-
663 MAVEN: A Fast, Robust, and User-Friendly Mass Spectrometry Data Processing Engine
664 for Metabolomics, in: D'Alessandro, A. (Ed.), High-Throughput Metabolomics, Methods
665 in Molecular Biology. Springer New York, New York, NY, pp. 301–321.
666 https://doi.org/10.1007/978-1-4939-9236-2_19
667 Alvarez-Jarreta, J., Amos, B., Aurrecoechea, C., Bah, S., Barba, M., Barreto, A., Basenko, E.Y.,
668 Belnap, R., Blevins, A., Böhme, U., Brestelli, J., Brown, S., Callan, D., Campbell, L.I.,
669 Christophides, G.K., Crouch, K., Davison, H.R., DeBarry, J.D., Demko, R., Doherty, R.,
670 Duan, Y., Dundore, W., Dyer, S., Falke, D., Fischer, S., Gajria, B., Galdi, D., Giraldo-
671 Calderón, G.I., Harb, O.S., Harper, E., Helb, D., Howington, C., Hu, S., Humphrey, J.,
672 Iodice, J., Jones, A., Judkins, J., Kelly, S.A., Kissinger, J.C., Kittur, N., Kwon, D.K.,
673 Lamoureux, K., Li, W., Lodha, D., MacCallum, R.M., Maslen, G., McDowell, M.A., Myers,
674 J., Nural, M.V., Roos, D.S., Rund, S.S.C., Shanmugasundram, A., Sitnik, V., Spruill, D.,
675 Starns, D., Tomko, S.S., Wang, H., Warrenfeltz, S., Wieck, R., Wilkinson, P.A., Zheng, J.,
676 2024. VEuPathDB: the eukaryotic pathogen, vector and host bioinformatics resource
677 center in 2023. Nucleic Acids Res 52, D808–D816.
678 https://doi.org/10.1093/nar/gkad1003
679 Amaratunga, C., Sreng, S., Suon, S., Phelps, E.S., Stepniewska, K., Lim, P., Zhou, C., Mao, S.,
680 Anderson, J.M., Lindegardh, N., Jiang, H., Song, J., Su, X., White, N.J., Dondorp, A.M.,
681 Anderson, T.J.C., Fay, M.P., Mu, J., Duong, S., Fairhurst, R.M., 2012. Artemisinin-resistant
682 Plasmodium falciparum in Pursat province, western Cambodia: a parasite clearance rate
683 study. Lancet Infect Dis 12, 851–858. https://doi.org/10.1016/S1473-3099(12)70181-0
684 Anaguano, D., Dedkhad, W., Brooks, C.F., Cobb, D.W., Muralidharan, V., 2023. Time-resolved
685 proximity biotinylation implicates a porin protein in export of transmembrane malaria
686 parasite effectors. J Cell Sci 136, jcs260506. https://doi.org/10.1242/jcs.260506
687 Aurrecoechea, C., Brestelli, J., Brunk, B.P., Dommer, J., Fischer, S., Gajria, B., Gao, X., Gingle, A.,
688 Grant, G., Harb, O.S., Heiges, M., Innamorato, F., Iodice, J., Kissinger, J.C., Kraemer, E., Li,
689 W., Miller, J.A., Nayak, V., Pennington, C., Pinney, D.F., Roos, D.S., Ross, C., Stoeckert,
690 C.J., Treatman, C., Wang, H., 2009. PlasmoDB: a functional genomic database for malaria
691 parasites. Nucleic Acids Res 37, D539-543. https://doi.org/10.1093/nar/gkn814
692 Bender, T., Pena, G., Martinou, J., 2015. Regulation of mitochondrial pyruvate uptake by
693 alternative pyruvate carrier complexes. The EMBO Journal 34, 911–924.
694 https://doi.org/10.15252/embj.201490197

695 Bonive-Boscan, A.D., Acosta, H., Rojas, A., 2023. Metabolic changes that allow *Plasmodium*
696 *falciparum* artemisinin-resistant parasites to tolerate the oxidative stress.
697 https://doi.org/10.1101/2023.10.21.560494
698 Bricker, D.K., Taylor, E.B., Schell, J.C., Orsak, T., Boutron, A., Chen, Y.-C., Cox, J.E., Cardon, C.M.,
699 Van Vranken, J.G., Dephoure, N., Redin, C., Boudina, S., Gygi, S.P., Brivet, M., Thummel,
700 C.S., Rutter, J., 2012. A mitochondrial pyruvate carrier required for pyruvate uptake in
701 yeast, Drosophila, and humans. Science 337, 96–100.
702 https://doi.org/10.1126/science.1218099
703 Bulusu, V., Jayaraman, V., Balaram, H., 2011. Metabolic fate of fumarate, a side product of the
704 purine salvage pathway in the intraerythrocytic stages of Plasmodium falciparum. J Biol
705 Chem 286, 9236–9245. https://doi.org/10.1074/jbc.M110.173328
706 Castegna, A., Scarcia, P., Agrimi, G., Palmieri, L., Rottensteiner, H., Spera, I., Germinario, L.,
707 Palmieri, F., 2010. Identification and functional characterization of a novel mitochondrial
708 carrier for citrate and oxoglutarate in Saccharomyces cerevisiae. J Biol Chem 285,
709 17359–17370. https://doi.org/10.1074/jbc.M109.097188
710 Chambers, M.C., Maclean, B., Burke, R., Amodei, D., Ruderman, D.L., Neumann, S., Gatto, L.,
711 Fischer, B., Pratt, B., Egertson, J., Hoff, K., Kessner, D., Tasman, N., Shulman, N., Frewen,
712 B., Baker, T.A., Brusniak, M.-Y., Paulse, C., Creasy, D., Flashner, L., Kani, K., Moulding, C.,
713 Seymour, S.L., Nuwaysir, L.M., Lefebvre, B., Kuhlmann, F., Roark, J., Rainer, P., Detlev, S.,
714 Hemenway, T., Huhmer, A., Langridge, J., Connolly, B., Chadick, T., Holly, K., Eckels, J.,
715 Deutsch, E.W., Moritz, R.L., Katz, J.E., Agus, D.B., MacCoss, M., Tabb, D.L., Mallick, P.,
716 2012. A cross-platform toolkit for mass spectrometry and proteomics. Nat Biotechnol
717 30, 918–920. https://doi.org/10.1038/nbt.2377
718 Chan, X.W.A., Wrenger, C., Stahl, K., Bergmann, B., Winterberg, M., Müller, I.B., Saliba, K.J.,
719 2013. Chemical and genetic validation of thiamine utilization as an antimalarial drug
720 target. Nat Commun 4, 2060. https://doi.org/10.1038/ncomms3060
721 Chen, N., LaCrue, A.N., Teuscher, F., Waters, N.C., Gatton, M.L., Kyle, D.E., Cheng, Q., 2014.
722 Fatty acid synthesis and pyruvate metabolism pathways remain active in
723 dihydroartemisinin-induced dormant ring stages of Plasmodium falciparum. Antimicrob
724 Agents Chemother 58, 4773–4781. https://doi.org/10.1128/AAC.02647-14
725 Claros, M.G., Vincens, P., 1996. Computational method to predict mitochondrially imported
726 proteins and their targeting sequences. Eur J Biochem 241, 779–786.
727 https://doi.org/10.1111/j.1432-1033.1996.00779.x
728 Cobbold, S.A., McConville, M.J., 2014. The Plasmodium Tricarboxylic Acid Cycle and
729 Mitochondrial Metabolism, in: Hommel, M., Kremsner, P.G. (Eds.), Encyclopedia of
730 Malaria. Springer New York, New York, NY, pp. 1–18. https://doi.org/10.1007/978-1-
731 4614-8757-9_13-1
732 Cobbold, S.A., Vaughan, A.M., Lewis, I.A., Painter, H.J., Camargo, N., Perlman, D.H.,
733 Fishbaugher, M., Healer, J., Cowman, A.F., Kappe, S.H., Llinas, M., 2013. Kinetic flux
734 profiling elucidates two independent acetyl-CoA biosynthetic pathways in Plasmodium
735 falciparum. The Journal of biological chemistry 288, 36338–50.
736 https://doi.org/10.1074/jbc.M113.503557

737 Cunningham, C.N., Rutter, J., 2020. 20,000 picometers under the OMM: diving into the vastness
738 of mitochondrial metabolite transport. EMBO Rep 21, e50071.
739 https://doi.org/10.15252/embr.202050071
740 de Vries, L.E., Jansen, P.A.M., Barcelo, C., Munro, J., Verhoef, J.M.J., Pasaje, C.F.A., Rubiano, K.,
741 Striepen, J., Abla, N., Berning, L., Bolscher, J.M., Demarta-Gatsi, C., Henderson, R.W.M.,
742 Huijs, T., Koolen, K.M.J., Tumwebaze, P.K., Yeo, T., Aguiar, A.C.C., Angulo-Barturen, I.,
743 Churchyard, A., Baum, J., Fernández, B.C., Fuchs, A., Gamo, F.-J., Guido, R.V.C., Jiménez-
744 Diaz, M.B., Pereira, D.B., Rochford, R., Roesch, C., Sanz, L.M., Trevitt, G., Witkowski, B.,
745 Wittlin, S., Cooper, R.A., Rosenthal, P.J., Sauerwein, R.W., Schalkwijk, J., Hermkens,
746 P.H.H., Bonnert, R.V., Campo, B., Fidock, D.A., Llinás, M., Niles, J.C., Kooij, T.W.A.,
747 Dechering, K.J., 2022. Preclinical characterization and target validation of the
748 antimalarial pantothenamide MMV693183. Nat Commun 13, 2158.
749 https://doi.org/10.1038/s41467-022-29688-5
750 Dondorp, A.M., Nosten, F., Yi, P., Das, D., Phyo, A.P., Tarning, J., Lwin, K.M., Ariey, F.,
751 Hanpithakpong, W., Lee, S.J., Ringwald, P., Silamut, K., Imwong, M., Chotivanich, K., Lim,
752 P., Herdman, T., An, S.S., Yeung, S., Singhasivanon, P., Day, N.P., Lindegardh, N., Socheat,
753 D., White, N.J., 2009. Artemisinin resistance in Plasmodium falciparum malaria. The New
754 England journal of medicine 361, 455–67. https://doi.org/10.1056/NEJMoa0808859
755 Gardner, M.J., Hall, N., Fung, E., White, O., Berriman, M., Hyman, R.W., Carlton, J.M., Pain, A.,
756 Nelson, K.E., Bowman, S., Paulsen, I.T., James, K., Eisen, J.A., Rutherford, K., Salzberg,
757 S.L., Craig, A., Kyes, S., Chan, M.-S., Nene, V., Shallom, S.J., Suh, B., Peterson, J., Angiuoli,
758 S., Pertea, M., Allen, J., Selengut, J., Haft, D., Mather, M.W., Vaidya, A.B., Martin, D.M.A.,
759 Fairlamb, A.H., Fraunholz, M.J., Roos, D.S., Ralph, S.A., McFadden, G.I., Cummings, L.M.,
760 Subramanian, G.M., Mungall, C., Venter, J.C., Carucci, D.J., Hoffman, S.L., Newbold, C.,
761 Davis, R.W., Fraser, C.M., Barrell, B., 2002. Genome sequence of the human malaria
762 parasite Plasmodium falciparum. Nature 419, 498–511.
763 https://doi.org/10.1038/nature01097
764 Harb, O.S., McDowell, M.A., Roos, D.S., 2024. VEuPathDB Resources: A Platform for Free Online
765 Data Exploration, Integration, and Analysis. Methods Mol Biol 2802, 573–586.
766 https://doi.org/10.1007/978-1-0716-3838-5_19
767 Herzig, S., Raemy, E., Montessuit, S., Veuthey, J.-L., Zamboni, N., Westermann, B., Kunji, E.R.S.,
768 Martinou, J.-C., 2012. Identification and Functional Expression of the Mitochondrial
769 Pyruvate Carrier. Science 337, 93–96. https://doi.org/10.1126/science.1218530
770 Hodge, T., Colombini, M., 1997. Regulation of metabolite flux through voltage-gating of VDAC
771 channels. J Membr Biol 157, 271–279. https://doi.org/10.1007/s002329900235
772 Homblé, F., Krammer, E.-M., Prévost, M., 2012. Plant VDAC: facts and speculations. Biochim
773 Biophys Acta 1818, 1486–1501. https://doi.org/10.1016/j.bbamem.2011.11.028
774 Ke, H., Lewis, I.A., Morrisey, J.M., McLean, K.J., Ganesan, S.M., Painter, H.J., Mather, M.W.,
775 Jacobs-Lorena, M., Llinás, M., Vaidya, A.B., 2015. Genetic investigation of tricarboxylic
776 acid metabolism during the Plasmodium falciparum life cycle. Cell Rep 11, 164–174.
777 https://doi.org/10.1016/j.celrep.2015.03.011
778 Liu, X., Cooper, D.E., Cluntun, A.A., Warmoes, M.O., Zhao, S., Reid, M.A., Liu, J., Lund, P.J.,
779 Lopes, M., Garcia, B.A., Wellen, K.E., Kirsch, D.G., Locasale, J.W., 2018. Acetate

780 Production from Glucose and Coupling to Mitochondrial Metabolism in Mammals. Cell
781 175, 502-513.e13. https://doi.org/10.1016/j.cell.2018.08.040
782 Lyu, C., Chen, Y., Meng, Y., Yang, J., Ye, S., Niu, Z., El-Debs, I., Gupta, N., Shen, B., 2023. The
783 Mitochondrial Pyruvate Carrier Coupling Glycolysis and the Tricarboxylic Acid Cycle Is
784 Required for the Asexual Reproduction of Toxoplasma gondii. Microbiol Spectr e05043-
785 22. https://doi.org/10.1128/spectrum.05043-22
786 MacRae, J.I., Dixon, M.W., Dearnley, M.K., Chua, H.H., Chambers, J.M., Kenny, S., Bottova, I.,
787 Tilley, L., McConville, M.J., 2013. Mitochondrial metabolism of sexual and asexual blood
788 stages of the malaria parasite Plasmodium falciparum. BMC Biol 11, 67.
789 https://doi.org/10.1186/1741-7007-11-67
790 Mallo, N., Ovciarikova, J., Martins-Duarte, E.S., Baehr, S.C., Biddau, M., Wilde, M.-L., Uboldi,
791 A.D., Lemgruber, L., Tonkin, C.J., Wideman, J.G., Harding, C.R., Sheiner, L., 2021.
792 Depletion of a Toxoplasma porin leads to defects in mitochondrial morphology and
793 contacts with the endoplasmic reticulum. J Cell Sci 134, jcs255299.
794 https://doi.org/10.1242/jcs.255299
795 Mok, S., Stokes, B.H., Gnädig, N.F., Ross, L.S., Yeo, T., Amaratunga, C., Allman, E., Solyakov, L.,
796 Bottrill, A.R., Tripathi, J., Fairhurst, R.M., Llinás, M., Bozdech, Z., Tobin, A.B., Fidock, D.A.,
797 2021. Artemisinin-resistant K13 mutations rewire Plasmodium falciparum's intra-
798 erythrocytic metabolic program to enhance survival. Nat Commun 12, 530.
799 https://doi.org/10.1038/s41467-020-20805-w
800 Nagampalli, R.S.K., Quesñay, J.E.N., Adamoski, D., Islam, Z., Birch, J., Sebinelli, H.G., Girard,
801 R.M.B.M., Ascenção, C.F.R., Fala, A.M., Pauletti, B.A., Consonni, S.R., de Oliveira, J.F.,
802 Silva, A.C.T., Franchini, K.G., Leme, A.F.P., Silber, A.M., Ciancaglini, P., Moraes, I., Dias,
803 S.M.G., Ambrosio, A.L.B., 2018. Human mitochondrial pyruvate carrier 2 as an
804 autonomous membrane transporter. Sci Rep 8, 3510. https://doi.org/10.1038/s41598-
805 018-21740-z
806 Nair, S.C., Munro, J.T., Mann, A., Llinás, M., Prigge, S.T., 2023. The mitochondrion of
807 Plasmodium falciparum is required for cellular acetyl-CoA metabolism and protein
808 acetylation. Proc Natl Acad Sci U S A 120, e2210929120.
809 https://doi.org/10.1073/pnas.2210929120
810 Nkrumah, L.J., Muhle, R.A., Moura, P.A., Ghosh, P., Hatfull, G.F., Jacobs, W.R., Fidock, D.A.,
811 2006. Efficient site-specific integration in Plasmodium falciparum chromosomes
812 mediated by mycobacteriophage Bxb1 integrase. Nat Methods 3, 615–621.
813 https://doi.org/10.1038/nmeth904
814 Nozawa, A., Fujimoto, R., Matsuoka, H., Tsuboi, T., Tozawa, Y., 2011. Cell-free synthesis,
815 reconstitution, and characterization of a mitochondrial dicarboxylate-tricarboxylate
816 carrier of Plasmodium falciparum. Biochem Biophys Res Commun 414, 612–617.
817 https://doi.org/10.1016/j.bbrc.2011.09.130
818 Painter, H.J., Morrisey, J.M., Mather, M.W., Vaidya, A.B., 2007. Specific role of mitochondrial
819 electron transport in blood-stage Plasmodium falciparum. Nature 446, 88–91.
820 https://doi.org/10.1038/nature05572
821 Peatey, C.L., Chavchich, M., Chen, N., Gresty, K.J., Gray, K.-A., Gatton, M.L., Waters, N.C., Cheng,
822 Q., 2015. Mitochondrial Membrane Potential in a Small Subset of Artemisinin-Induced

823 Dormant Plasmodium falciparum Parasites In Vitro. J Infect Dis 212, 426–434.
824 https://doi.org/10.1093/infdis/jiv048
825 Pédelacq, J.-D., Cabantous, S., Tran, T., Terwilliger, T.C., Waldo, G.S., 2006. Engineering and
826 characterization of a superfolder green fluorescent protein. Nat Biotechnol 24, 79–88.
827 https://doi.org/10.1038/nbt1172
828 Pei, Y., Tarun, A.S., Vaughan, A.M., Herman, R.W., Soliman, J.M.B., Erickson-Wayman, A., Kappe,
829 S.H.I., 2010. Plasmodium pyruvate dehydrogenase activity is only essential for the
830 parasite's progression from liver infection to blood infection. Mol Microbiol 75, 957–
831 971. https://doi.org/10.1111/j.1365-2958.2009.07034.x
832 Prata, I.O., Cubillos, E.F.G., Krüger, A., Barbosa, D., Martins, J., Setubal, J.C., Wunderlich, G.,
833 2021. Plasmodium falciparum Acetyl-CoA Synthetase Is Essential for Parasite
834 Intraerythrocytic Development and Chromatin Modification. ACS Infect Dis 7, 3224–
835 3240. https://doi.org/10.1021/acsinfecdis.1c00414
836 Rajaram, K., Liu, H.B., Prigge, S.T., 2020. Redesigned TetR-Aptamer System To Control Gene
837 Expression in Plasmodium falciparum. mSphere 5.
838 https://doi.org/10.1128/mSphere.00457-20
839 Rajaram, K., Tewari, S.G., Wallqvist, A., Prigge, S.T., 2022. Metabolic changes accompanying the
840 loss of fumarate hydratase and malate–quinone oxidoreductase in the asexual blood
841 stage of Plasmodium falciparum. Journal of Biological Chemistry 298, 101897.
842 https://doi.org/10.1016/j.jbc.2022.101897
843 Roberts, A.D., Nair, S.C., Guerra, A.J., Prigge, S.T., 2019. Development of a conditional
844 localization approach to control apicoplast protein trafficking in malaria parasites.
845 Traffic 20, 571–582. https://doi.org/10.1111/tra.12656
846 Rocamora, F., Zhu, L., Liong, K.Y., Dondorp, A., Miotto, O., Mok, S., Bozdech, Z., 2018. Oxidative
847 stress and protein damage responses mediate artemisinin resistance in malaria
848 parasites. PLoS Pathog 14, e1006930. https://doi.org/10.1371/journal.ppat.1006930
849 Schalkwijk, J., Allman, E.L., Jansen, P.A.M., de Vries, L.E., Verhoef, J.M.J., Jackowski, S., Botman,
850 P.N.M., Beuckens-Schortinghuis, C.A., Koolen, K.M.J., Bolscher, J.M., Vos, M.W., Miller,
851 K., Reeves, S.A., Pett, H., Trevitt, G., Wittlin, S., Scheurer, C., Sax, S., Fischli, C., Angulo-
852 Barturen, I., Jiménez-Diaz, M.B., Josling, G., Kooij, T.W.A., Bonnert, R., Campo, B.,
853 Blaauw, R.H., Rutjes, F.P.J.T., Sauerwein, R.W., Llinás, M., Hermkens, P.H.H., Dechering,
854 K.J., 2019. Antimalarial pantothenamide metabolites target acetyl–coenzyme A
855 biosynthesis in *Plasmodium falciparum*. Sci. Transl. Med. 11, eaas9917.
856 https://doi.org/10.1126/scitranslmed.aas9917
857 Schwach, F., Bushell, E., Gomes, A.R., Anar, B., Girling, G., Herd, C., Rayner, J.C., Billker, O.,
858 2015. PlasmoGEM, a database supporting a community resource for large-scale
859 experimental genetics in malaria parasites. Nucleic Acids Res 43, D1176-1182.
860 https://doi.org/10.1093/nar/gku1143
861 Shi, L., Tu, B.P., 2015. Acetyl-CoA and the regulation of metabolism: mechanisms and
862 consequences. Curr Opin Cell Biol 33, 125–131.
863 https://doi.org/10.1016/j.ceb.2015.02.003
864 Storm, J., Perner, J., Aparicio, I., Patzewitz, E.-M., Olszewski, K., Llinas, M., Engel, P.C., Müller, S.,
865 2011. Plasmodium falciparum glutamate dehydrogenase a is dispensable and not a drug

target during erythrocytic development. Malar. J. 10, 193. https://doi.org/10.1186/1475-2875-10-193

Storm, J., Sethia, S., Blackburn, G.J., Chokkathukalam, A., Watson, D.G., Breitling, R., Coombs, G.H., Müller, S., 2014. Phosphoenolpyruvate carboxylase identified as a key enzyme in erythrocytic Plasmodium falciparum carbon metabolism. PLoS Pathog 10, e1003876. https://doi.org/10.1371/journal.ppat.1003876

Summers, R.L., Pasaje, C.F.A., Pisco, J.P., Striepen, J., Luth, M.R., Kumpornsin, K., Carpenter, E.F., Munro, J.T., Lin, D., Plater, A., Punekar, A.S., Shepherd, A.M., Shepherd, S.M., Vanaerschot, M., Murithi, J.M., Rubiano, K., Akidil, A., Ottilie, S., Mittal, N., Dilmore, A.H., Won, M., Mandt, R.E.K., McGowen, K., Owen, E., Walpole, C., Llinás, M., Lee, M.C.S., Winzeler, E.A., Fidock, D.A., Gilbert, I.H., Wirth, D.F., Niles, J.C., Baragaña, B., Lukens, A.K., 2021. Chemogenomics identifies acetyl-coenzyme A synthetase as a target for malaria treatment and prevention. Cell Chem Biol S2451-9456(21)00350–0. https://doi.org/10.1016/j.chembiol.2021.07.010

Swift, R.P., Rajaram, K., Keutcha, C., Liu, H.B., Kwan, B., Dziedzic, A., Jedlicka, A.E., Prigge, S.T., 2020a. The NTP generating activity of pyruvate kinase II is critical for apicoplast maintenance in Plasmodium falciparum. Elife 9, e50807. https://doi.org/10.7554/eLife.50807

Swift, R.P., Rajaram, K., Liu, H.B., Dziedzic, A., Jedlicka, A.E., Roberts, A.D., Matthews, K.A., Jhun, H., Bumpus, N.N., Tewari, S.G., Wallqvist, A., Prigge, S.T., 2020b. A mevalonate bypass system facilitates elucidation of plastid biology in malaria parasites. PLoS Pathog 16, e1008316. https://doi.org/10.1371/journal.ppat.1008316

Swift, R.P., Rajaram, K., Liu, H.B., Prigge, S.T., 2021. Dephospho-CoA kinase, a nuclear-encoded apicoplast protein, remains active and essential after Plasmodium falciparum apicoplast disruption. EMBO J 40, e107247. https://doi.org/10.15252/embj.2020107247

Tavoulari, S., Thangaratnarajah, C., Mavridou, V., Harbour, M.E., Martinou, J.-C., Kunji, E.R., 2019. The yeast mitochondrial pyruvate carrier is a hetero-dimer in its functional state. EMBO J 38, e100785. https://doi.org/10.15252/embj.2018100785

Tripathi, J., Stoklasa, M., Nayak, S., Low, K.E., Lee, E.Q.H., Rénia, L., Malleret, B., Bozdech, Z., 2023. The artemisinin-induced dormant stages of *Plasmodium falciparum* exhibit hallmarks of cellular senescence and drug resilience. https://doi.org/10.1101/2023.01.29.526019

van Dooren, G.G., Stimmler, L.M., McFadden, G.I., 2006. Metabolic maps and functions of the Plasmodium mitochondrion. FEMS Microbiol Rev 30, 596–630. https://doi.org/10.1111/j.1574-6976.2006.00027.x

van Esveld, S.L., Meerstein-Kessel, L., Boshoven, C., Baaij, J.F., Barylyuk, K., Coolen, J.P.M., van Strien, J., Duim, R.A.J., Dutilh, B.E., Garza, D.R., Letterie, M., Proellochs, N.I., de Ridder, M.N., Venkatasubramanian, P.B., de Vries, L.E., Waller, R.F., Kooij, T.W.A., Huynen, M.A., 2021. A Prioritized and Validated Resource of Mitochondrial Proteins in Plasmodium Identifies Unique Biology. mSphere 6, e0061421. https://doi.org/10.1128/mSphere.00614-21

Wang, J., Huang, L., Li, J., Fan, Q., Long, Y., Li, Y., Zhou, B., 2010. Artemisinin directly targets malarial mitochondria through its specific mitochondrial activation. PLoS One 5, e9582. https://doi.org/10.1371/journal.pone.0009582

910 Weiner, J., Kooij, T.W.A., 2016. Phylogenetic profiles of all membrane transport proteins of the
911 malaria parasite highlight new drug targets. Microb Cell 3, 511–521.
912 https://doi.org/10.15698/mic2016.10.534
913 Wideman, J.G., Gawryluk, R.M.R., Gray, M.W., Dacks, J.B., 2013. The ancient and widespread
914 nature of the ER-mitochondria encounter structure. Mol Biol Evol 30, 2044–2049.
915 https://doi.org/10.1093/molbev/mst120
916 Witkowski, B., Amaratunga, C., Khim, N., Sreng, S., Chim, P., Kim, S., Lim, P., Mao, S., Sopha, C.,
917 Sam, B., Anderson, J.M., Duong, S., Chuor, C.M., Taylor, W.R.J., Suon, S., Mercereau-
918 Puijalon, O., Fairhurst, R.M., Menard, D., 2013. Novel phenotypic assays for the
919 detection of artemisinin-resistant Plasmodium falciparum malaria in Cambodia: in-vitro
920 and ex-vivo drug-response studies. Lancet Infect Dis 13, 1043–1049.
921 https://doi.org/10.1016/S1473-3099(13)70252-4
922 Witkowski, B., Lelièvre, J., Barragán, M.J.L., Laurent, V., Su, X., Berry, A., Benoit-Vical, F., 2010.
923 Increased tolerance to artemisinin in Plasmodium falciparum is mediated by a
924 quiescence mechanism. Antimicrob. Agents Chemother. 54, 1872–1877.
925 https://doi.org/10.1128/AAC.01636-09
926 World Health Organization, 2023. World malaria report 2023. World Health Organization,
927 Geneva.
928 Wunderlich, J., 2022. Updated List of Transport Proteins in Plasmodium falciparum. Front Cell
929 Infect Microbiol 12, 926541. https://doi.org/10.3389/fcimb.2022.926541
930 Yang, M., Ke, H., Morrisey, J.M., Mather, M.W., Vaidya, A.B., 2022. Genetic disruption of
931 isocitrate dehydrogenase arrests the full development of sexual stage parasites in
932 *Plasmodium falciparum*. https://doi.org/10.1101/2022.08.05.502965
933 Yu, X., Wang, C., Zhao, Y., Tang, J., Zhu, M., Platon, L., Culleton, R., Zhu, G., Ménard, D., Zhang,
934 Q., Cao, J., 2023. Ring-stage growth arrest: Metabolic basis of artemisinin tolerance in
935 Plasmodium falciparum. iScience 26, 105725.
936 https://doi.org/10.1016/j.isci.2022.105725
937 Zhang, H., Guo, J., Li, H., Guan, Y., 2022. Machine learning for artemisinin resistance in malaria
938 treatment across in vivo-in vitro platforms. iScience 25, 103910.
939 https://doi.org/10.1016/j.isci.2022.103910
940 Zhang, M., Wang, C., Otto, T.D., Oberstaller, J., Liao, X., Adapa, S.R., Udenze, K., Bronner, I.F.,
941 Casandra, D., Mayho, M., Brown, J., Li, S., Swanson, J., Rayner, J.C., Jiang, R.H.Y., Adams,
942 J.H., 2018. Uncovering the essential genes of the human malaria parasite Plasmodium
943 falciparum by saturation mutagenesis. Science 360, eaap7847.
944 https://doi.org/10.1126/science.aap7847
945 Zhu, L., van der Pluijm, R.W., Kucharski, M., Nayak, S., Tripathi, J., White, N.J., Day, N.P.J., Faiz,
946 A., Phyo, A.P., Amaratunga, C., Lek, D., Ashley, E.A., Nosten, F., Smithuis, F., Ginsburg,
947 H., von Seidlein, L., Lin, K., Imwong, M., Chotivanich, K., Mayxay, M., Dhorda, M.,
948 Nguyen, H.C., Nguyen, T.N.T., Miotto, O., Newton, P.N., Jittamala, P., Tripura, R.,
949 Pukrittayakamee, S., Peto, T.J., Hien, T.T., Dondorp, A.M., Bozdech, Z., 2022. Artemisinin
950 resistance in the malaria parasite, Plasmodium falciparum, originates from its initial
951 transcriptional response. Commun Biol 5, 274. https://doi.org/10.1038/s42003-022-
952 03215-0
953